UNIVERSITATEA BABEȘ-BOLYAI

Facultatea de Fizică

Școala Doctorală de Fizică

TEZĂ DE DOCTORAT
ABSTRACT

Modern methods of analysis of materials of biological origin

Lavinia Raluca DRĂGAN (căs. ȘAITIȘ)

Conducător științific

Prof. Dr. Radu FECHETE

CONTAINED

INTRODUCTION

Colorectal cancer is the second most common cancer in the world and has aggressive malignancy, with a high tendency to deep invasion, lymph node metastases, and distant metastases [1]. Due to its frequent diagnosis, usually only at an advanced stage, the reported incidence of colon cancer increases remarkably each year. In the year 2020, colorectal cancer ranked third as the most common type of cancer diagnosed worldwide, with approximately 1.9 million new cases and causing 930,000 deaths. Epidemiological projections indicate that by the year 2040, the incidence of this type of cancer will increase significantly, reaching about 3.2 million new cases annually, while associated mortality is expected to increase to 1.6 million deaths per year [2]. It also holds the second position in cancer-related deaths and is the main contributor to cancer-related deaths in men under 50 years of age. More than half of all colorectal cancer cases can be attributed to modifiable risk factors such as tobacco use, an unhealthy eating pattern, excessive alcohol consumption, lack of physical activity, and obesity [3]. A substantial number of cases of colorectal cancer and mortality can be avoided through regular *screening*, vigilant monitoring and access to high-quality medical care [4]. *Serum markers* (indicators) such as carcinoembryonic antigen (CEA) and cancerous antigen 19-9 (CA 19-9) have low specificity and sensitivity [5]. Colonoscopy, one of the most available diagnostic methods, has a high degree of invasiveness [6].

The main objective of this doctoral thesis is to use relaxometry and diffusiometry measurements of 1H MRI in low magnetic fields, high-resolution 1H MRI spectroscopy as well as FT-IR spectroscopy, for the identification of specific characteristics sensitive to the presence of features (*markers)* colorectal cancer in native and deproteinised blood plasma and blood plasma proteins, as well as MRI spectroscopy and imaging in high magnetic fields to characterise healthy tissues or tissues affected by colorectal cancer or other materials of biological origin. For this, the raw data are analyzed by numerical procedures involving the deconvolution (of the FT-IR spectra) and the inverse Laplace transform (of the fall curves of the type CPMG and PGSE by MRI of 1H) to obtain the distributions of the transverse relaxation time, *T2* and the self-diffusion coefficient D . The relevant parameters were used as input data for the PCA analyses and the most important physical properties (the parameters describing the physical systems studied), blood samples or biopsies taken from colorectal cancer patients or from samples taken from healthy volunteers are identified.

CHAPTER 1 Physiology of Blood

General

Blood is a fundamental component of human life [7] made up of several types of components with very diverse properties and is often called a *liquid organ* [8]. In the body of an adult, about 4 to 5 liters of blood circulates continuously through a complex network of vessels, propelled by the strong contractions of the beating heart [7], and its distribution, through the vascular system, throughout the body is essential for the existence of the body [8].

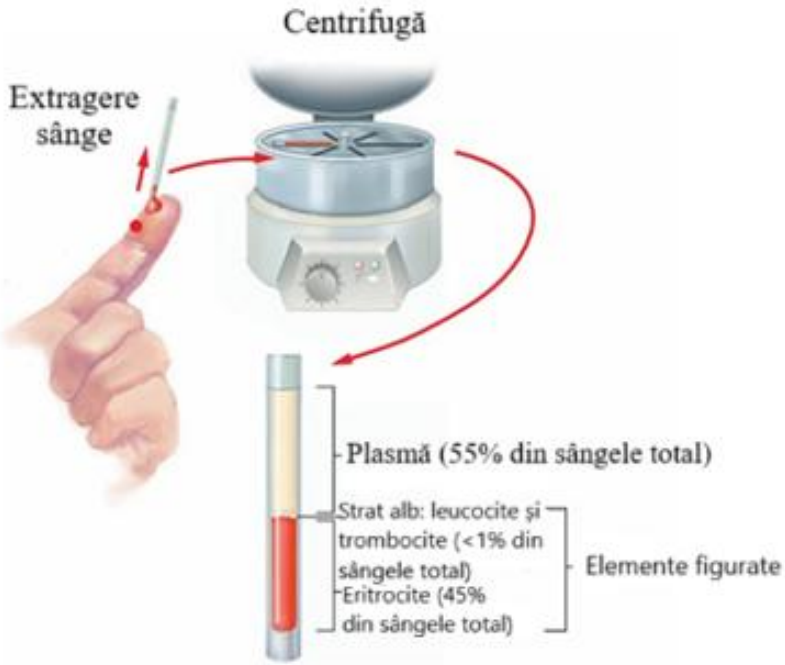

Fig. 1.1 A small blood sample is collected in a biochemistry tube and centrifuged to separate the plasma cells [after reference 9].

1.2 Blood components

Blood is made up of two main parts, namely blood cells [8] which are also called figurative elements [10] and which are synthesized mainly in bone marrow and blood plasma, or the liquid part of blood [8]. The figured elements can be separated from the plasma by placing a blood sample in a tube and centrifuging it for several minutes. Because red blood cells are denser than blood plasma, they are deposited at the base of the tube and usually make up about 45% of the total volume. This value is referred to as hematocrit. The white blood cells and platelets form a thin, cream-colored area called the leukocyte layer, located just above the red blood cells. At the top of the tube is plasma, which is pale yellow in colour and accounts for almost 55 % of the total volume [9].

1.2.1 Colorectal cancer

Colorectal cancer (CRC) is one of the most common types of cancer in Western countries and, increasingly, globally [11]. It is the second leading cause of cancer death worldwide [12], and the most common in both sexes [13, 14], with cancer taking nearly one million lives in 2020 [12]. There are several modifiable risk factors associated with CRC, and in the case of well-defined hereditary syndromes, which include CRC as a manifestation, germline genetic mutations have been identified. Polyps, especially adenomas, are recognized preneoplastic lesions, and their accessibility through endoscopy allows both early detection and effective diagnosis and treatment [11]. Over the course of a lifetime, the risk of developing colorectal cancer (hereinafter referred to as CRC or CRC) in patients at average risk is about 5%, and in 90% of cases, the disease occurs after the age of 50. Unfortunately, almost a third of people diagnosed with CRC die from this condition. Although the early forms of the disease are often curable by surgery, in the advanced stages, when metastases are present and surgical treatment is no longer an option, the prognosis becomes severe and the course is fatal. These aspects underline the importance of effective screening and monitoring programmes, which are essential for the early detection of the disease. In addition, identifying and managing premalignant lesions is a crucial step in preventing the development of colorectal cancer [13].

Risk factors for colorectal cancer are both genetic and environmental in nature, and they play a key role in determining how the disease presents itself, being classified into three types: sporadic, inherited and familial. Sporadic cases, in which there is no family history of cancer, account for about 70% of all CRC cases. Usually, patients with this form are older than 50 years old, and the etiological factors involved are those related to diet and the environment. However, genetic changes have also been identified that lead to the progression of the disease from adenoma to carcinoma [15]. In less than 10% of patients, there is an inherited genetic predisposition for CRC, and these cases can be divided according to the presence or absence of colon polyps as the main manifestation. Polyposis diseases include familial adenomatous polyposis (FAP) and hamartomatous polyposis syndromes such as Peutz-Jeghers syndrome and juvenile polyposis [16], while non-polyposis diseases are hereditary non-polyposis colorectal cancer (also known as Lynch I syndrome) and familial cancer syndrome (Lynch II syndrome) [17]. The third type of colorectal cancer, the least understood to date, is known as familial colorectal cancer. Almost 25% of affected patients have a family history of colorectal cancer, but their pattern (structure) does not correspond to those described in the aforementioned inherited syndromes. People from these families have a higher risk of developing colorectal cancer.

1.3 Methods of separation of blood components

The separation of blood components is an essential step in biochemical and metabolic analysis, being necessary for investigating plasma composition and identifying relevant metabolites in various pathologies [18].

Stages I - Processing of blood samples

a) *Sampling from patients.* Blood samples are taken under aseptic conditions, using the venipuncture technique. A disposable needle and a vacuum or syringe collection system are used.

b) *Transfer of blood to the test tube.* The collected blood is immediately distributed in specific test tubes, depending on the type of analysis required. Biochemistry test tubes without anticoagulant are used to obtain the serum.

c) *Preparing the test tube for spinning.* The test tubes are inverted several times for blood homogenization and are then placed in a suitable holder, ready for centrifugation. Tubes without anticoagulant are left to stand at room temperature for 30–60 minutes.

d) *Centrifugation of samples.* The test tubes are placed in a balanced centrifuge, with tightly closed lids, and are subjected to centrifugation according to the protocol. The centrifugation parameters vary depending on the desired component, as follows: i) For plasma separation: 2000–3000 rpm for 10–15 minutes at 4°C; ii) Separation of blood fractions.

e) *Following centrifugation*, the samples are separated into distinct fractions: i) Plasma or serum – the clear, upper layer used for biochemical and metabolomic analyses; ii) Buffy coat – the intermediate, whitish layer containing leukocytes and platelets (used for DNA isolation or immunological analysis) and iii) Figurative elements (erythrocytes, leukocytes, platelets) – the lower, compacted layer.

f) *Plasma/serum collection.* The plasma or serum is carefully extracted using a micropipette or automatic pipette, without disturbing the buffy coat or erythrocyte mass. The sample is transferred to sterile tubes and stored at the appropriate temperature (-80 °C for long-term storage or 4 °C for immediate analysis).

Steps II - Processing of plasma samples

a) *Transfer of plasma into microtubes (Eppendorf).* The plasma obtained after the initial centrifugation is transferred using a micropipette to a sterile Eppendorf microtube, ensuring gentle handling of the sample to avoid contamination or hemolysis.

b) *Plasma sampling for protein precipitation.* A 100 µL volume of plasma is precisely pipetted and transferred to a 1.5 mL Eppendorf microtube for the deproteinization step.

c) *Adding solvent for protein precipitation.* In the same Eppendorf microtube, 900 µL of cold methanol is added to obtain a 1:9 plasma/methanol ratio, favorable to protein precipitation. The mixture is homogenized by gentle vortexing for a few seconds. *Preparation of samples for centrifugation.* The Eppendorf microtubes containing the plasma-methanol mixture are placed in a larger test tube (15 or 50 mL, depending on the centrifuge configuration) to ensure rotor balancing and mechanical protection of the samples during centrifugation.

d) *Introduction of microtubes into the centrifuge.* The microtubes are symmetrically distributed in the centrifuge rotor to prevent mechanical imbalance. Check the correct positioning and close the centrifuge lid.

e) *Centrifugation for separation of plasma fractions.* The centrifugation of the samples is performed at 4°C, at a relative centrifugal force (RCF) of 2000 g, for 10-15 minutes. This process causes the precipitated proteins (which are deposited at the bottom of the microtube) to separate from the clear supernatant.

f) *Separation of supernatant from precipitate.* After centrifugation, the samples are handled carefully to avoid resuspension of the protein precipitate. The supernatant (clear liquid layer) is separated with a micropipette and transferred to a new, sterile Eppendorf microtube.

g) *Supernatant collection (deproteinized plasma).* The supernatant, which contains soluble metabolites and other non-protein components, is retained for further analysis, such as MRI spectroscopy or FT-IR spectroscopy. It can be stored temporarily at -20 °C or long-term at -80 °C to prevent degradation of volatile compounds.

h) *The resulting protein sediment.* The protein precipitate, visible as a whitish deposit at the base of the microtube, can be removed or used for further proteomic analysis if necessary.

CHAPTER 2 METHODS OF ANALYSIS AND MATERIAL RESOURCES

2.1 Nuclear magnetic resonance

2.1.1 General principles

Spectroscopy is an advanced method of studying various types of materials that provides detailed information based on examining the specific way matter interacts with electromagnetic radiation. Atoms and molecules are known to exhibit a series of discrete energy levels, which correspond to the electronic, vibrational or rotational states that are quantized. The interaction occurs through the absorption and emission of photons (in the visible domain or adjacent domains), where the energy of the photons matches the energy difference between two energy states. Because the energy of a photon (generally of a radiation quantum) is directly related to its frequency. Thus, the different types of spectroscopy are usually defined based on the frequencies of the specific electromagnetic radiation involved in the interaction process. The processes of absorption and emission of radiation lead to transitions between the electronic states of the outer electrons and usually involve frequencies in the ultraviolet (UV) range, leading to UV spectroscopy. Molecular vibration modes are characterized by frequency values just below those of red light in the visible range and are thus analyzed using infrared (IR) spectroscopy. Otherwise, nuclear magnetic resonance spectroscopy (NMR for short) uses frequencies in the radio wave range, usually in the range of 10 to 1000 MHz [19].

2.1.2 NMR proton relaxometry

The CPMG (Carr-Purcell-Meiboom-Gill) pulse sequence is widely used in the world, especially when using MRI relaxometry techniques, to rapidly obtain (*single shoot*) MRI signal drops that contain information about molecular dynamics on a time scale covering several orders of magnitude and that are suitable for characterizing most liquid and soft solid organic samples or biological tissues. The fall of the train of multiple echoes that occur in the CPMG in measurements made in homogeneous, or even inhomogeneous, magnetic fields is generated by a combination of stimulated echoes and Hahn.

Multi-exponential analysis of CPMG data

In recent years, various algorithms have been developed that more or less efficiently perform the inverse Laplace transform of experimental data [20, 21-25]. This is a badly conditioned problem so the data must be regularized to make the effects of noise. To date, the inverse Laplace transform has been applied in NMR mostly for isolated spine systems such as fluids in porous media [21-23, 26, 27] or food samples [27] and free-to-diffuse molecules [22, 24, 26-28].

A data inversion algorithm (by inverse Laplace-type transform) was described in references [21, 29] was used in the experimental part of this thesis for data processing and obtaining a normalized distribution of the transverse relaxation time *T2*, which is denoted by *f*(*T2*) and is related to the magnetization of the spin system by,

$$M(\tau) = \int_0^\infty f(T_2) e^{-\frac{\tau}{T_2}} dT_2, \quad (2.1)$$

2.1.3 Localized high-field 1H MRI spectroscopy

Nuclear magnetic resonance spectroscopy is possible for any nucleus that possesses a magnetic moment (the nuclear spin must be non-zero). For in *vivo* applications of magnetic resonance spectroscopy, metabolic nuclei with a high degree of interest that have this property are proton (^{1}H), carbon-13 (^{13}C), phosphorus (^{31}P) and sodium (^{23}Na). Although the number of relevant nuclei is limited, each nucleus provides a large amount of information, as a large number of metabolites can be detected simultaneously. Magnetic resonance spectroscopy of ^{1}H allows the detection of important neurotransmitters, such as glutamate, GABA or aspartate, together with related compounds, such as glutamine, and the end product of glycolysis, lactate. ^{13}C offers the possibility to study *in vivo* but non-invasively complex flows through important metabolic pathways, such as the tricarboxylic acid cycle. ^{31}P spectroscopy provides information on energy-important metabolites, intracellular pH, magnesium concentration and reaction flows. In addition to the mentioned nuclei, MRS magnetic resonance spectroscopy or *in vivo* may also become relevant for other nuclei in special cases, such as helium (^{3}He), lithium (^{7}Li), nitrogen (^{15}N), oxygen (^{17}O), fluorine (^{19}F), silicon (^{29}Si) and potassium (^{39}K) [19].

2.2 Spectroscopia FT-IR

2.2.1 General principles

Fourier transform infrared spectroscopy (FT-IR) is a widely used technique for identifying functional groups in materials, whether gaseous, liquid or solid, using infrared (IR) radiation. Infrared spectroscopy measures the absorption of IR radiation by each bond in a molecule, resulting in a spectrum usually represented as absorbance (dimensionless) or transmittance (%) versus wavenumber (cm^{-1}). A variety of covalently bonded materials absorb electromagnetic radiation in the IR region, which has a lower energy and longer wavelength than light (visible range electromagnetic radiation) or UV radiation (which are used together in UV-VIS spectroscopy), but a higher energy and shorter wavelength than microwave radiation. In order for a molecule to be identified by its functional groups using IR spectroscopy, it must be active in IR,

i.e. it must have a dipole moment (non-zero). When IR radiation interacts with the covalent bonds of materials that have an electric dipole, the molecule absorbs energy, causing the chemical bond to oscillate. This oscillation, which modifies the net dipole moment of the molecule, is what allows the absorption of IR radiation [30]. The interaction of electromagnetic radiation with the substance is expressed in two ways: i) by the absorption, emission or dispersion of electromagnetic waves, and ii) by temporary or permanent changes in the optical, magnetic, thermal or chemical properties of the substance, regardless of whether it is made up of atoms, molecules, ions or other chemical entities [31]. The interaction of substances with any part of the electromagnetic spectrum is called spectroscopy, which is an analysis between matter and electromagnetic radiation in any field. The electromagnetic spectrum is made up of several types of radiation that include various wavelengths, being a form of radiant energy, starting from gamma rays and X-rays, passing through UV radiation, visible light, infrared, microwave and up to radio waves, each of which can be seen as a wave or particle that moves at the speed of light.

2.3 Material resource

In order to carry out this study, a close collaboration was carried out with the medical team from the Surgery I Department, which contributed to the collection of biological samples, ensuring adequate storage conditions and maintaining their integrity until the sampling and processing stage in order to obtain the final form for analysis.

2.3.1 Patients with colorectal cancer

In this study, all patients provided written informed consent, being fully informed about the objectives of the research and the specific procedures for collecting biological samples. The selection of patients diagnosed with colorectal cancer was based on a diagnosis confirmed by high-resolution imaging, including pelvic magnetic resonance imaging (MRI) and echo-endoscopy. For studies I and II, a total of 31 patients with histopathologically confirmed diagnosis, aged 35 to 81 years, were included. The exclusion criteria targeted patients who required emergency surgery. The study was conducted at the Cluj-Napoca County Clinical Hospital, Surgery I Department.

2.3.2 Healthy volunteers

Similar to patients diagnosed with colorectal cancer, volunteers in the control group received and signed informed consent to participate in the study. The criteria for inclusion in this group have been rigorously defined to ensure an appropriate comparison with the patient group. Thus, participants in the control group did not have a diagnosis of colorectal cancer, had ages and gender distribution comparable to those of cancer patients, and had no history of significant gastrointestinal disorders such as Crohn's disease, ulcerative colitis, advanced polyps, or

predisposing genetic syndromes, such as Lynch syndrome. Individuals with a history of pre-existing neoplastic diseases were also excluded.

Table 2.1 Some extensive characteristics (label, age, sex, environment of origin, RCT – radiochemically treated, diagnosis, histological grade, cancer staging, pn – regional lymph nodes) specific to patients with colorectal cancer.

PATIENTS WITH COLORECTAL CANCER									
Nr. crt.	**Label patient**	**Age**	**Sex**	**Environ-ment of origin**	**RCT**	**Diagnostic**	**Degree histologic**	**Staging Cancer**	**pn (regional lymph nodes)**
1	C031	35	F	RURAL	RCT	ADK COLONIC TRANSVERS	G2	T3N0M1	5N+/41
2	C032	56	M	URBAN	RCT	ADK COLONIC TRANSVERS	G2	T3N0M1	15N0
3	C036	57	M	URBAN	RCT	ADK COLONIC MIJLOCIU	G1	T2N0M0	22N+/32
4	C041	61	M	URBAN	RCT	ADK COLONIC ASCENDENT	G2	T3N0M0	15N0
5	C042	77	M	RURAL	RCT	ADK COLONIC ASCENDENT	G2	T3N0M0	28N0
6	C045	54	M	URBAN	RCT	ADK COLONIC ASCENDENT	G2	T3N0M1	23N0
7	C059	65	M	RURAL	RCT	ADK COLONIC SIGMOID	G2	T3N0M0	25N0
8	C060	50	F	RURAL	RCT	ADK COLONIC SIGMOID	G2	T2N0M0	3N+/3N0
9	C067	60	M	URBAN	RCT	ADK COLONIC SIGMOID	G2	T2N0M0	15N0
10	C074	60	M	RURAL	NU	ADK COLONIC ASCENDENT	G1	T1N0M0	X
11	C075	70	F	URBAN	RCT	ADK colonic mijlociu	G1	T1N0M0	NO
12	C081	43	M	URBAN	RCT	ADK COLONIC MIJLOCIU	G3	T3N3M1	4N+/12N
13	C098	67	M	URBAN	RCT	ADK COLONIC ASCENDENT	G2	T3N2M0	
14	C100	74	F	URBAN	RCT	ADK RECTAL mucinos	G3	T2N1bM0	2N+/17
15	C101	68	M	URBAN	RCT	ADK sigmoid	G2	T3N0M0	8N0
16	C102	54	F	URBAN	NU	ADK colonic transvers	G2	T2N0M0	(0/45)N0
17	C103	68	F	URBAN	NU	ADK colonic nos moderat diferențiat	G2	T3N1cM0	(0/16)N0
18	C104	67	M	URBAN	NU	Adenocarci-nom rectal moderat diferențiat	G2	T2N0M0	17N0
19	C105	55	M	URBAN	RCT	ADK SIGMOID	G2	T4N1M0	10N0
20	C0106	60	M	RURAL	RCT	ADK SIGMOID	G2	T2N0M0	6N0

21	C107	80	M	RURAL	NU	ADK colonic de tip mucinos	G2	T4bN2M1	2+/8
22	C108	64	M	URBAN	NU	ADK TRANS-VERS colonic bine/moderat diferentiat	G2	T3N0M0	12N0
23	C110	46	F	URBAN	NU	Adenocarci-nom tubular de colon de-scendent	G2	T4bN3M1	5+/10
24	C111	59	F	URBAN	NU	Adenocarci-nom bine diferentiat	G1	T3N0M0	18N0
25	C112	85	B	URBAN	NU	Adenocarciom colonic mode-rat diferentiat	G2	T4N1M1	5+/5
26	C123	78	B	RURAL	NU	Adenocarci-nom colonic moderat diferentiat	G2	T2N0M0	15N0
27	C136	72	F	URBAN	NU	Adenocarci-nom cecal, bine diferentiat	G1	T2N0M0	17N0
28	C137	72	F	URBAN	RCT	ADK COLONIC cec	G2	T3N1M0	15N0
29	C140	46	B	RURAL	NU	Adenocarci-nom colon sig-moid	G2	T3N0M0	31N0
30	C141	63	F	URBAN	NU	Adenocarci-nom colonic moderat diferentiat	G2	T4aN1bM0.	N1+
31	C147	67	F	URBAN	NU	Adenocarci-nom colonic moderat diferentiat	G2	T3N0Mo	12N0

Table 2.2 Some characteristics (label, age, gender, background) of healthy volunteers.

VOLUNTARI SĂNĂTOȘI				
Nr.crt	Patient label	Age	Sex	Environment of origin
1	V01	53	M	URBAN

2	V02	50	M	URBAN
3	V03	49	M	RURAL
4	V04	53	F	URBAN
5	V05	60	F	URBAN
6	V06	34	F	URBAN
7	V07	51	F	URBAN
8	V08	42	F	URBAN
9	V09	49	F	RURAL
10	V10	25	M	RURAL
11	V11	39	M	RURAL
12	V12	74	M	URBAN
13	V13	49	M	URBAN
14	V14	30	M	RURAL
15	V15	55	F	URBAN
16	V16	46	M	RURAL
17	V17	36	M	URBAN
18	V18	44	M	URBAN
19	V19	50	M	URBAN
20	V20	56	F	URBAN

CHAPTER 3 CHARACTERIZATION OF BLOOD PLASMA BY RELAXOMETRY AND DIFFUSION MRI

3.1 Pilot Study 1

3.1.1 Distributions of spin-spin relaxation times, T_2

Blood has two major plasma components that contain more than 90% water and blood cells. This component is well reflected in specific relaxation times. Figure 3.1 shows the distributions of T2 transverse relaxation times measured for blood plasma collected from three healthy volunteers and 7 colorectal cancer patients. In Figure 3.1a, a number of four peaks can be observed. *The main peak* is located at a T2 value of slightly less than 1 s, which indicates that the largest amount of 1H is found in the water in the blood plasma. The center and width of this *peak* are affected by dissolved substances. This is indicated by the fact that the T2 value is less than 2 s compared to the 3 s characteristic of distilled water. In addition to this main *peak*, there are three other secondary peaks located at i) about 0.9 to 1.3 ms that are associated with relatively immobile components; ii) another *peak* located at approximately 3.4 – 4.1 ms, which is associated with components with reduced mobility; and iii) another *peak* located at approximately 14.2 – 17.6 ms, which may be associated with components with medium mobility. *The main peak* is not very well defined. It has an asymmetrical shape and presents, at higher T2 values, an elongated tail. Thus, the echo time (TE) value of 70 μs that was used in the CPMG pulse sequence must be increased. A different value of the echo time (TE = 0.5 ms) was used, and that resulted in two effects. First, an increased TE value will have a filtering effect on components with a shorter relaxation time (see Figure 3.1b). Therefore, it can be seen that components with relaxation times around 1 ms disappear. Secondly, a better definition of the main *peaks* located at about 731 - 771 ms is observed, and what was the desired effect. There is a great similarity between the distributions of *T2* measured for the three volunteers, as the values of *T2* differ slightly. Figure 3.1c shows the distributions of relaxation times obtained using the inverse Laplace transform of the CPMG signal drop curves measured with an echo time of 70 ms, for a number of seven patients with colorectal cancer. A main peak can also be observed, located at *T2 values* below one second, between ~581 ms to 761 ms. Again, for a more accurate measurement of the position of the main peak, a second set of measurements were made with an echo time of 0.50 ms, and the corresponding distributions are shown in Figure 3.1d. Visually, no major changes are observed when comparing the transverse relaxation time (*T2* distributions) measured in the native blood plasma of cancer patients with those measured for healthy volunteers.

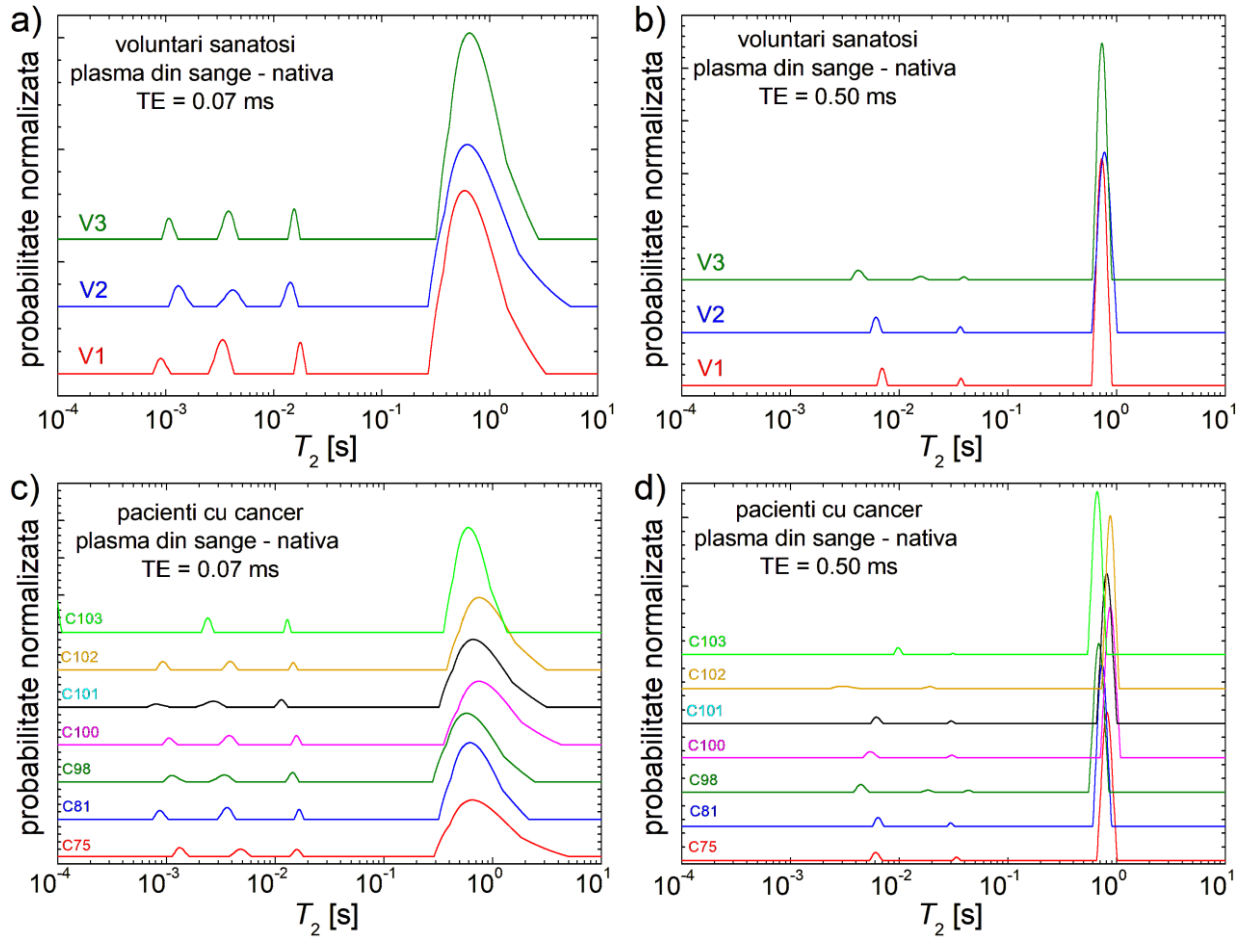

Fig.3.1. T_2 relaxation time distributions measured for native blood plasma harvested from V1-V3 healthy volunteers (top, a and b) and colorectal cancer patients (bottom – c and d) with echo time of TE = 70 μs (left) and TE = 500 μs = 0.50 ms (right).

3.1.2 Distributions of the self-diffusion coefficient, D

The self-diffusion coefficient of blood molecules (especially water molecules) is an important parameter even in clinical trials, for example for MRI imaging weighted with the average (apparent) self-diffusion coefficient (ADC). The distributions of the self-diffusion coefficient, *D* measured for native blood plasma, are shown in Figure 3.2. For the three volunteers (V1, V2 and V3) the distribution of *D* is shown in Figure 3.2a, while Figure 3.2b shows the distributions measured for the seven samples of native blood plasma belonging to patients with colorectal cancer. In all cases, the appearance of two or more peaks can be observed, one of them being the main peak located from about 2.52×10-9 m2/s to ~4.31×10-9 m2/s and another lower peak (or two *peaks* in the case of volunteer V1) is at high values of *D*. In principle, the main peaks are associated with relatively free water molecules.

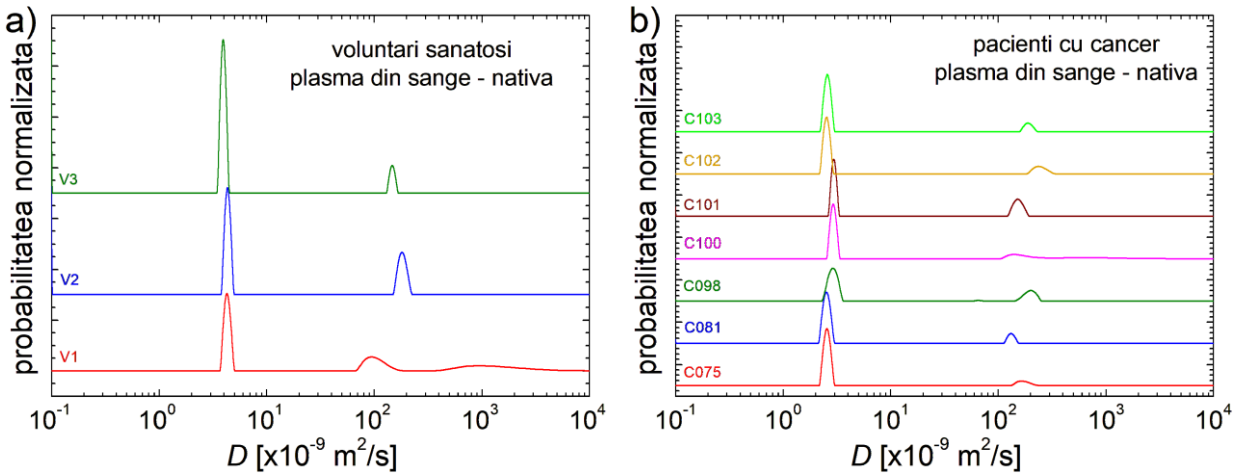

Fig. 3.2. The distribution of self-diffusion coefficient *D* measured by MRI of 1H for a) healthy volunteers and b) patients with colorectal cancer.

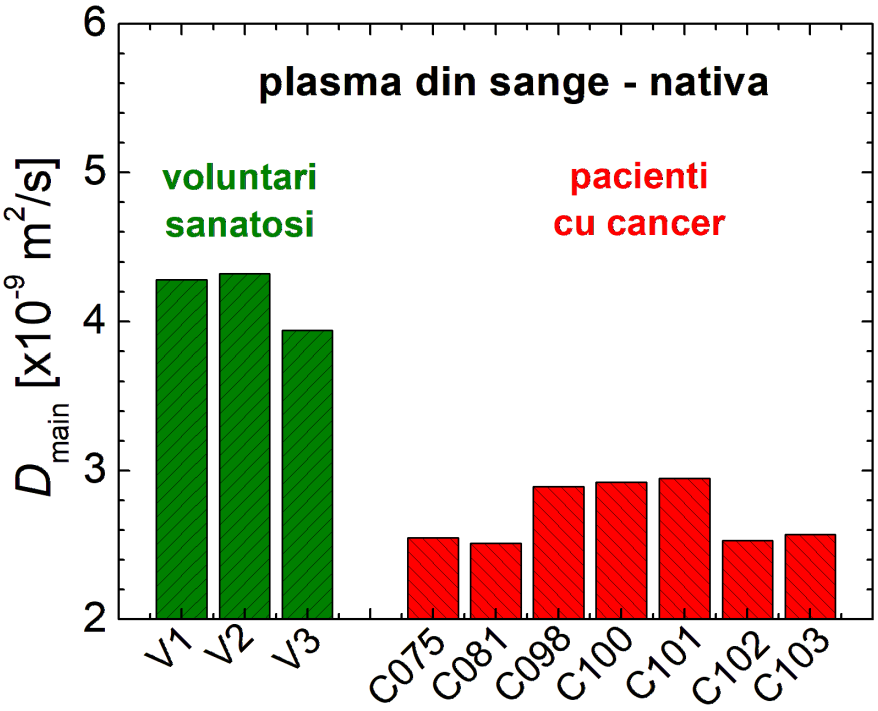

Fig. 3.3. Values of the 1H self-diffusion principal (*main*) coefficient measured by MRI for healthy volunteers (V1-V3) and colorectal cancer patients (C31-C103)

In our case, for blood plasma belonging to healthy volunteers, these peaks are located at values higher than 3.9×10-9 m2/s as read in Figure 3.2a. Lower D-values are observed measured from the position of the main *peaks* for cancer patients (see Figure 3.2b). More precise measurements of the maximum of these main peaks are shown in Figure 3.3. For healthy volunteers, three measurements can be observed at values above 3.9×10-9 m2/s (3.94, 4.28 and 4.32×10-9 m2/s). In contrast, for cancer patients, the highest value (at which the maximum distribution of the main peak is obtained) *Dmain* has values lower than 2.95×10-9 m2/s.

CHAPTER 4 CHARACTERIZATION OF BLOOD PLASMA BY FT-IR SPECTROSCOPY

4.1 Pilot Study 1

4.1.1 FT-IR spectra for native plasma

Fourier transformation infrared spectroscopy (FT-IR) is a powerful method for identifying compounds in samples to be studied. Thus, by analyzing FT-IR spectra, information related to the chemical bonds of specific biomarkers can be obtained [32]. Figure 4.1a shows the comparative FT-IR spectra measured for the blood plasma of healthy volunteers. It can be seen that FT-IR spectra are relatively simple. Thus, in the range of 3000-4000 $^{cm-1}$, a high peak *is observed* , with a large integrated area, which can be associated mainly with water in the blood plasma. There is also a small and wide peak centered around 2085 $^{cm-1}$. In the range of specific frequencies, which are usually associated with characteristic functional groups (from 350 to about 1800 $^{cm-1}$), there are found (see Figures 4.2): i) a *high peak*, with a large integrated area, centered around 1644 $^{cm-1}$ associated with Amida I; ii) a small peak centered around 1552 $^{cm-1}$ associated with Amida II; iii) a series of peaks small bands, which are centred at 1461 $^{cm-1}$, 1400 $^{cm-1}$ and which can be associated with the symmetrical stretching of COO- belonging to glutamate and aspartate-like amino acids and with the symmetrical bending modes of methyl, CH3 groups in proteins; iv) a very small and wide peak, centred around 1243 $^{cm-1}$ associated with asymmetrical stretching; v) a wide band centred around 567-577 $cmPO_2^{-1}$, which is usually neglected in the analysis of blood plasma specific to patients with colorectal cancer [32].

In the most important aspects, it can be said that the spectra recorded for healthy volunteers are similar to each other.

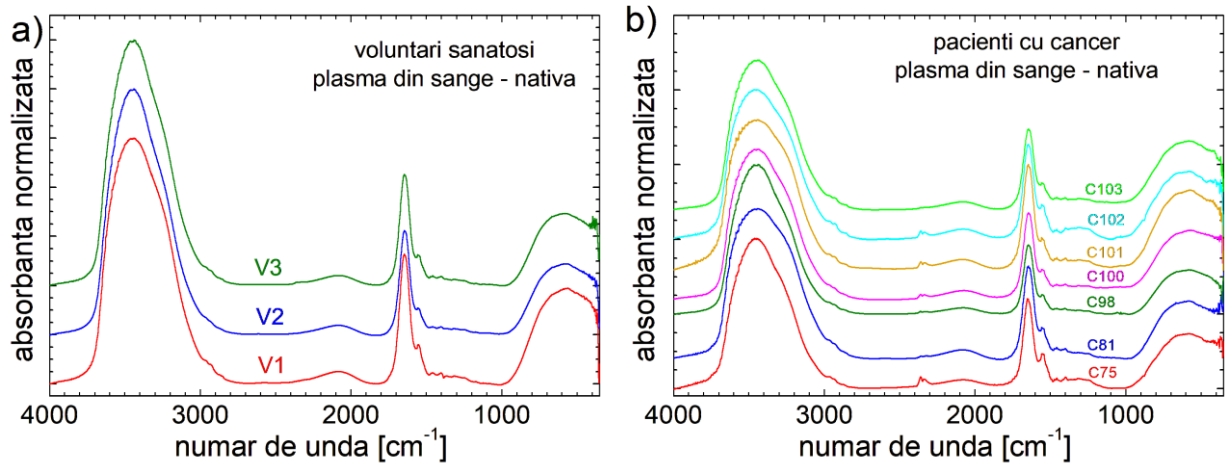

Fig. 4.1. Blood plasma FT-IR spectra measured for a) healthy volunteers (V1-V3) and b) colorectal cancer patients (C75-C103).

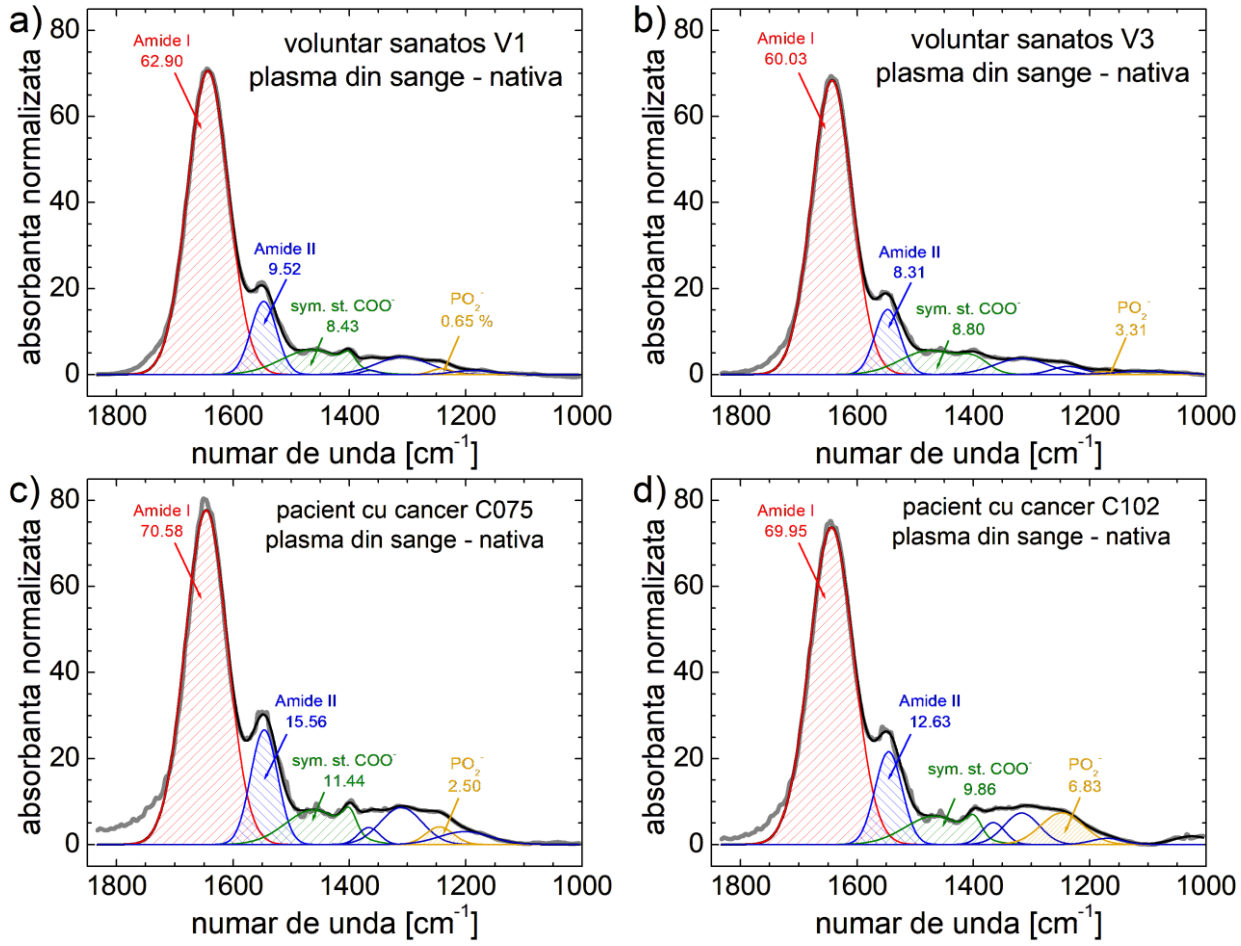

Fig. 4.2 Deconvolution of FT-IR spectra measured for native plasma collected from healthy volunteers a) V1 and b) V3 and for colorectal cancer patients c) C075 and d) C102. The integral area corresponding to Amide I, Amide II extends symmetrically from COO- and are shown.$\boldsymbol{PO_2^-}$

4.1.2 FT-IR spectra for deproteinized plasma

The FT-IR spectra recorded for deproteinised blood plasma collected from healthy volunteers are shown in Figure 4.3a. The deproteinization process takes place in the presence of methyl alcohol, which is why the FT-IR spectrum has some specific characteristics. In these cases, it can be said that the FT-IR spectra measured for the deproteinized blood plasma of the three volunteers are similar. The FT-IR spectra measured for the deproteinized blood plasma of the seven colorectal cancer patients are shown in Figure 4.3b. The specific associations of these peaks for the FT-IR spectrum shown in Figure 4.4 have been detailed in subchapter 4.1.1.

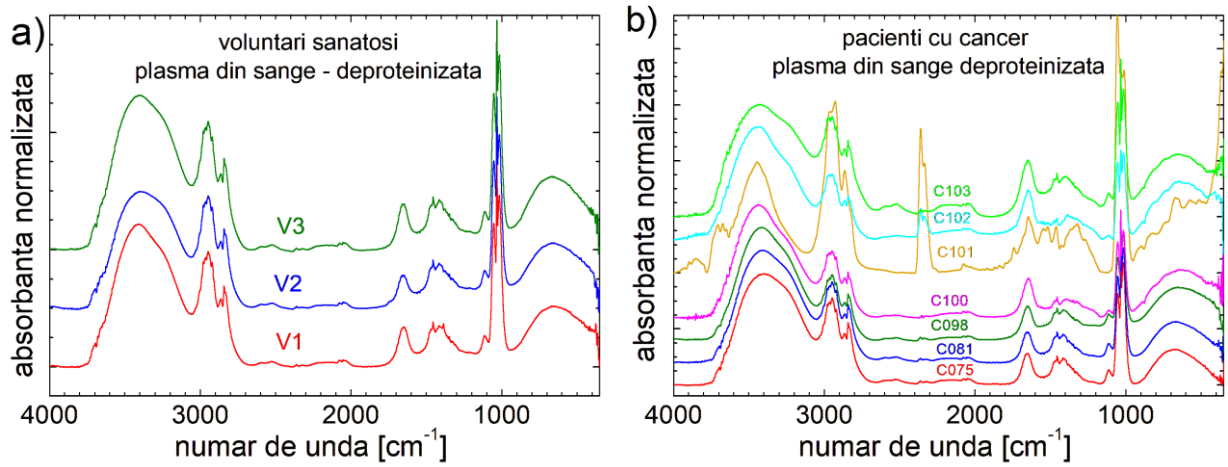

Fig. 4.3. FT-IR spectra of deproteinized blood plasma measured a) healthy volunteers (V1-V3) and b) colorectal cancer patients (C75-C103).

CHAPTER 5 ASSESSMENT OF HEALING 7 DAYS AFTER SURGERY

5.1 Specific preoperative and postoperative medical data

For this study, we used data from a group of 20 healthy volunteers, aged between 26 and 65 years (mean age was 52 years), with no history of cancer, and 10 patients diagnosed with colorectal cancer (both men and women), aged between 45 and 81 years (mean age being 67.6 years).

Several variables were considered, including age, neoadjuvant treatment, weight, diabetes, anaemia, Rayan score, haemoglobin levels before and after the seven days, among others, and these data are presented in Table 5.1. A key aspect of the study was the Rayan score, which is determined based on histopathological analysis and can last between four and six weeks. This was a crucial indicator, as it allowed the correlation of the results obtained by MRI methods and FT-IR spectroscopy, thus validating the accuracy and applicability of these techniques. Below in table 5.1 are presented all the data collected from the 10 patients with colorectal cancer.

Table 5.1 Social and clinical parameters of the patients studied (P1 to P10) [33].

Pacient	P1	P2	P3	P4	P5	P6	P7	P8	P9	P10
Sex	F	M	M	M	M	M	F	M	F	M
Varstă	45	67	66	67	81	67	72	81	55	75
Mediul de origine	urban	urban	rural	urban	urban	urban	urban	urban	urban	urban
Diagnostic ADK	Mediu/ inferior -Rectal	Jos - Rectal	Colon Sigmoid	Colon mucinos de grad scăzut	Jos - Rectal	Colorec-tal moderat diferențiat	Rectal moderat diferențiat	colo-rectal	Colo-rectal moderat diferențiat	Colon diferen-tiat
PET-CT/CT	PET-CT	CT	CT	CT	CT	CT	CT	CT	CT	CT
Tratament neoadjuvant	RCT	RCT	RCT	NU	RCT	NU	RCT	NU	NU	NU
Fumat	NU	DA	DA	NU	NU	DA	NU	NU	DA	DA
Categorii IMC	Greutate normală	Greutate scăzută	Greutate scăzută	Greutate scăzută	Greutate normală	Greutate normală	Greutate scăzută	Greutate normală	Greutate scăzută	Greutate scăzută
Histologie	G2	G1	G2	G2	G2	G2	G2	G1	G2	G1
Stadiul diagnosticu-lui după operație	I	II	IV	III	0	III	I	I	III	III
Pierderea poftei de mâncare	DA	DA	DA	DA	NU	DA	DA	NU	DA	DA
Pierderea în greu-tate	DA	DA	DA	DA	DA	DA	DA	DA	DA	DA
Febră	NU	NU	NU	DA	NU	NU	NU	NU	NU	NU
Sângerare rectală	DA	DA	NU	NU	DA	DA	DA	DA	DA	DA
Tulburări de tranzit intestinal	DA	DA	DA	DA	DA	DA	DA	DA	DA	DA
Consumul de alcool	NU	RAR	DA	NU	RAR	RAR	NU	RAR	RAR	RAR

Diabet	dz tip II	NU	NU	dz tip II	NU	dz tip II	NU	NU	NU	NU
Anemie	NU	NU	DA	NU	DA	NU	NU	NU	DA	da
Hemoroizi	interni	NU	NU	NU	interni	interni	interni & ex-terni	interni	NU	interni
Sideremie (μg/dL)	82	113	25	30	40	60	67	33	10	8
Hg preoperator (g/dL)	13.5	15.9	10.5	13.3	10.2	13.0	12.5	13.4	8.9	7.9
Hg 7 days (g/dL) postoperator (fL).	12.5	13.5	10.2	12.2	9.9	12.9	10.5	11.3	11.6	10.7
RDW-SD preopera-tor (fL)	49.9	45.8	48.4	53.2	46.8	45.4	48.3	54	79.3	44.1
RDW-SD at 7 days postoperator	47	43.1	53.8	51.1	45.6	45.5	47.3	53.2	89.9	66.4
Scor Rayan	1	3	-	-	0	-	3	-	-	-

5.2 Comparative analysis of native plasma in the blood by MRI relaxometry methods

Transverse relaxation time distributions, *T2* measured for native blood plasma collected from P1 to P5 patients with colorectal cancer presented as a pair of preoperative (red) and postoperative 7 days postoperatively (green) are shown in Fig. 5.1; while the distributions of *T2* measured for patients from P6 to P10 are shown in Figure 5.2. The measurements were made with two echo times (TE = 70 μs – left and TE = 500 μs – right). The experimental values were thus chosen to observe *the peaks that occur at a small T2 relaxation time (low TE) and to clarify the peaks that occur at high T2 values* (high TE). A small echo time, TE will artificially widen *the peaks that occur at* high T2 values, *while a high TE value will filter out rapidly falling MRI signal components (low* T2 values). As a general remark, four peaks can be observed: i) three of them located at *T2* values below 20 ms (for TE = 0.07 ms) and ii) one, the main peak, located at *T2* values greater than 600 ms (see the figures on the right with TE = 0.5 ms). From left to right (i.e., from *lower T2* values to higher values), *peaks* describe components of native blood plasma (containing $^{1H)}$ with increasing mobility. These components can be referred to as rigid, semi-rigid, intermediate, and mobile. As expected, the largest amount of 1H is localized in the most mobile components, most likely water in the blood plasma. Distilled water peaks in *the T2 distribution* at about 3 s. If some dissolved fractions are present in the water, then the corresponding *peak* is shifted to lower *T2* values [33].

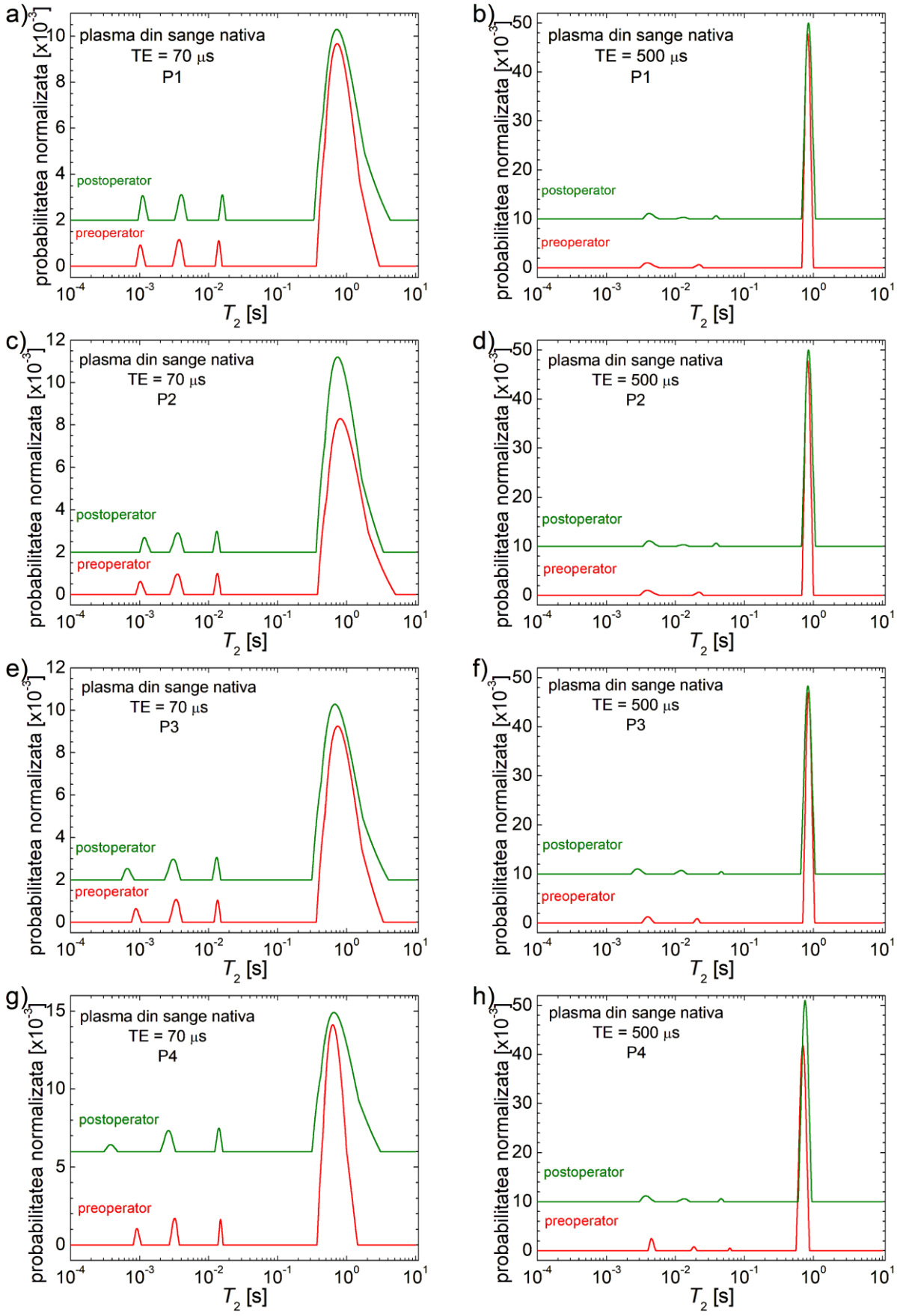
a)
plasma din sange nativa
TE = 70 μs
P1
postoperator
preoperator
probabilitatea normalizata [x10^{-3}]
T_2 [s]
b)
plasma din sange nativa
TE = 500 μs
P1
postoperator
preoperator
probabilitatea normalizata [x10^{-3}]
T_2 [s]
c)
plasma din sange nativa
TE = 70 μs
P2
postoperator
preoperator
probabilitatea normalizata [x10^{-3}]
T_2 [s]
d)
plasma din sange nativa
TE = 500 μs
P2
postoperator
preoperator
probabilitatea normalizata [x10^{-3}]
T_2 [s]
e)
plasma din sange nativa
TE = 70 μs
P3
postoperator
preoperator
probabilitatea normalizata [x10^{-3}]
T_2 [s]
f)
plasma din sange nativa
TE = 500 μs
P3
postoperator
preoperator
probabilitatea normalizata [x10^{-3}]
T_2 [s]
g)
plasma din sange nativa
TE = 70 μs
P4
postoperator
preoperator
probabilitatea normalizata [x10^{-3}]
T_2 [s]
h)
plasma din sange nativa
TE = 500 μs
P4
postoperator
preoperator
probabilitatea normalizata [x10^{-3}]
T_2 [s]

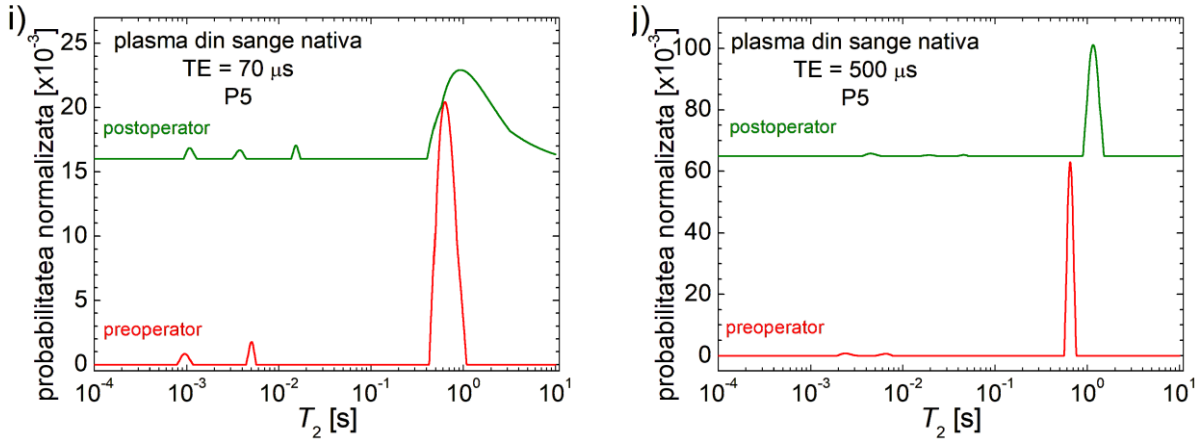

Fig. 5.1 T2 distributions measured with two values of echo onset time, TE = 70 μs and 500 μs for native blood plasma collected from patients a) and b) P1; c) and d) P2; e) and f) P3; g) and h) P4; i) and j) P5; with preoperative (red) and postoperative colorectal cancer 7 days after surgery (green).

5.3 Comparative analysis of blood plasma by FT-IR spectroscopy methods

Unlike ^{1}H MRI relaxometry, where the Laplace-type spectra (*T2 distributions*) are interpreted according to the position of the peaks correlated with the molecular dynamics influenced by the components (soluble and insoluble fractions), in the case of Fourier transform infrared spectroscopy (FT-IR), the concentration of a specific component (the vibration of the molecular bond occurring at a well-defined wavenumber) is directly proportional to the the amplitude of the measured peak. In this situation, FT-IR spectra measured for native and deproteinized blood plasma collected from 20 healthy volunteers could be mediated. These FT-IR spectra are shown in Figure 5.2 for native blood plasma. and for deproteinised plasma (blue line), together with FT-IR spectra measured for deproteinised plasma collected preoperatively (red) and postoperatively (green). Compared to the FT-IR spectra measured for deproteinized plasma, those measured for native plasma are simpler (see Fig. 5.2). A number of 5 distinct regions can be noted [247]: i) a wide *peak* between approx. 350 – 1000 $^{cm-1}$; ii) a region with low absorbance between about 1000 – 1500 $^{cm-1}$; iii) a narrow *peak* with the right shoulder between approx. 1500 – 1800 $^{cm-1}$; iv) a wide *peak* with low amplitude between about 1850 – 2500 $^{cm-1}$ and v) a *peak* between approximately 2700 – 3800 $^{cm-1}$.

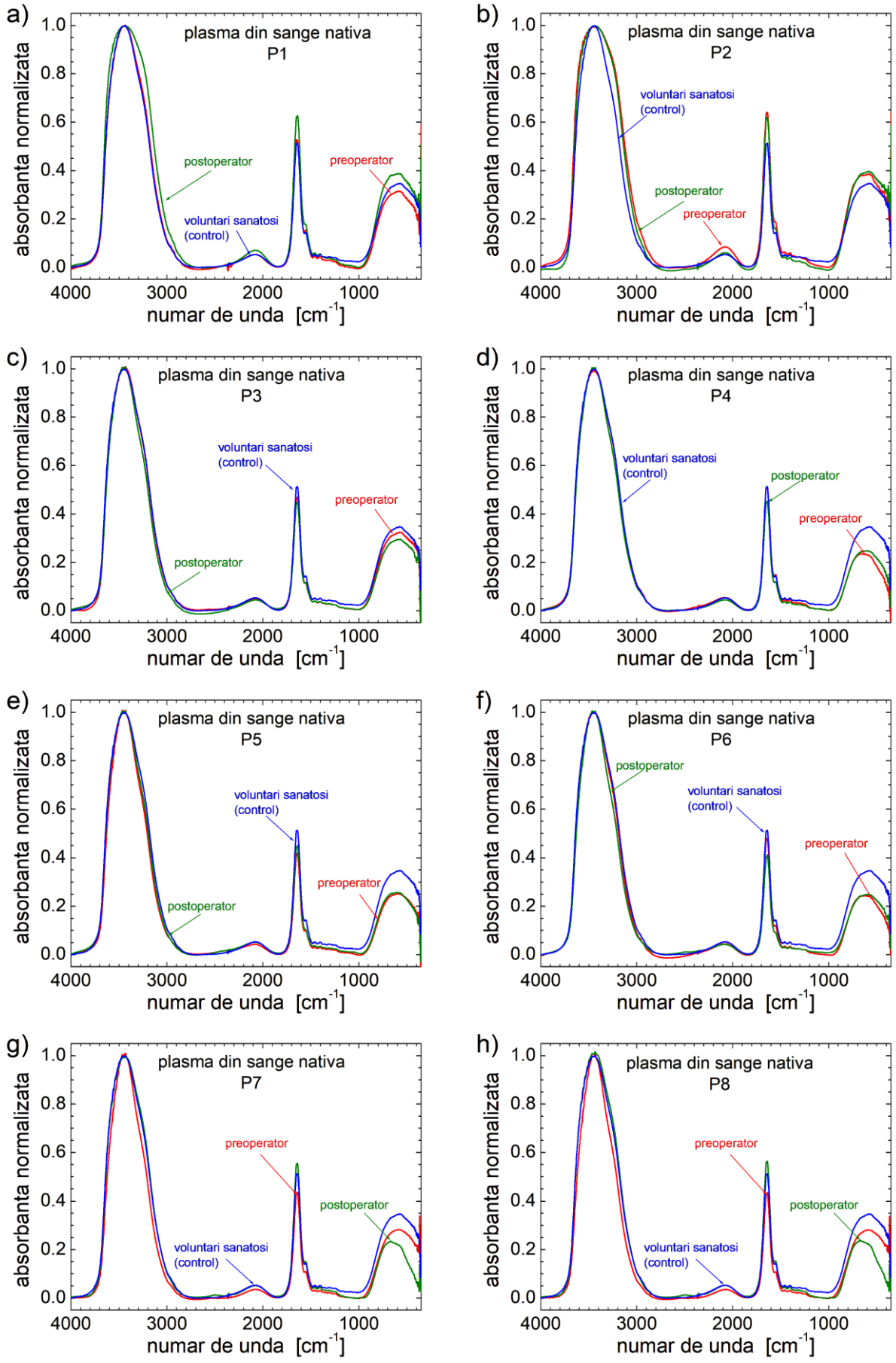
a)
plasma din sange nativa
P1
postoperator
preoperator
voluntari sanatosi
(control)
b)
plasma din sange nativa
P2
voluntari sanatosi
(control)
postoperator
preoperator
c)
plasma din sange nativa
P3
voluntari sanatosi
(control)
preoperator
postoperator
d)
plasma din sange nativa
P4
voluntari sanatosi
(control)
postoperator
preoperator
e)
plasma din sange nativa
P5
voluntari sanatosi
(control)
preoperator
postoperator
f)
plasma din sange nativa
P6
postoperator
voluntari sanatosi
(control)
preoperator
g)
plasma din sange nativa
P7
preoperator
postoperator
voluntari sanatosi
(control)
h)
plasma din sange nativa
P8
preoperator
postoperator
voluntari sanatosi
(control)
absorbanta normalizata
numar de unda [cm-1]
1.0
0.8
0.6
0.4
0.2
0.0
4000
3000
2000
1000

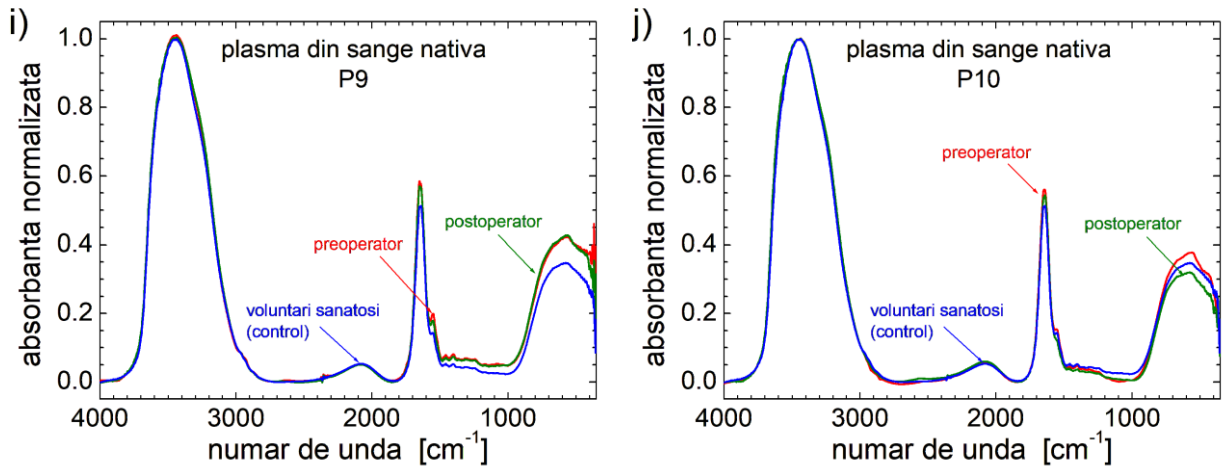

Fig. 5.2 FT-IR spectra measured for native blood plasma collected from patients a) P1, b) P2; (c) P3, (d) P4; (e) P5, (f) P6; (g) P7, (h) P8; i) P9 and j) P10; with preoperative (red) and postoperative colorectal cancer at 7 days postoperatively (green) compared to FT-IR spectra mediated for 20 healthy volunteers.

CHAPTER 6 PRINCIPAL COMPONENT STATISTICAL ANALYSIS OF SPECIFIC PARAMETERS FOR THE IDENTIFICATION OF METABOLITES IN BLOOD PLASMA AND ARTIFICIAL INTELLIGENCE

6.1 PCA Analysis Used for Identification of Colorectal Cancer in Blood Plasma Using Fourier Transform Infrared Spectroscopy (FT-IR) Measurements and Relaxometry and Nuclear Magnetic Resonance Diffusion of 1H

6.1.1 Specific parameters for PCA analysis

From a practical point of view, the distributions generated by MRI of the T2 transverse relaxation time and the self-diffusion coefficient *D*, but especially the FT-IR spectra, present some characteristic features that are not so easy to quantify for a definitive classification in the category of healthy volunteers or patients with colorectal cancer. Indeed, in the pilot study presented in chapters 3 and 4 it was possible to identify such features as the appearance of a small *peak* for all colorectal cancer patients in the *T2* distributions measured for deproteinized blood plasma, or the main value of the self-diffusion coefficient, *Dmain* which was found in a range (below 2.95×10-9 m2/s) for colorectal cancer patients and in another range (over 3.9×10-9 m2/s) for healthy volunteers, but these are generally particular cases. Thus, for a statistical analysis, it is often necessary that the measured data be prepared for this purpose.

Apart from age and the main value of the self-diffusion coefficient, *Dmain* a numerical deconvolution procedure applied to FT-IR spectra can lead to another set of quantifiable parameters. Thus, for example, Figure 6.1 shows FT-IR spectra measured for two healthy volunteers (see Figures 6.1a and 6.1b) and two patients with colorectal cancer (see Figures 6.1c

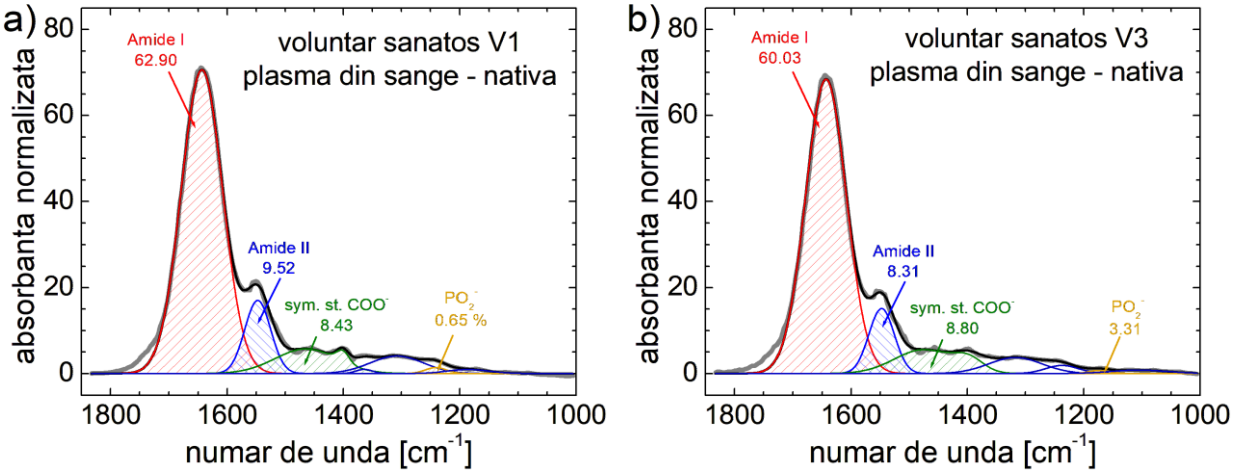

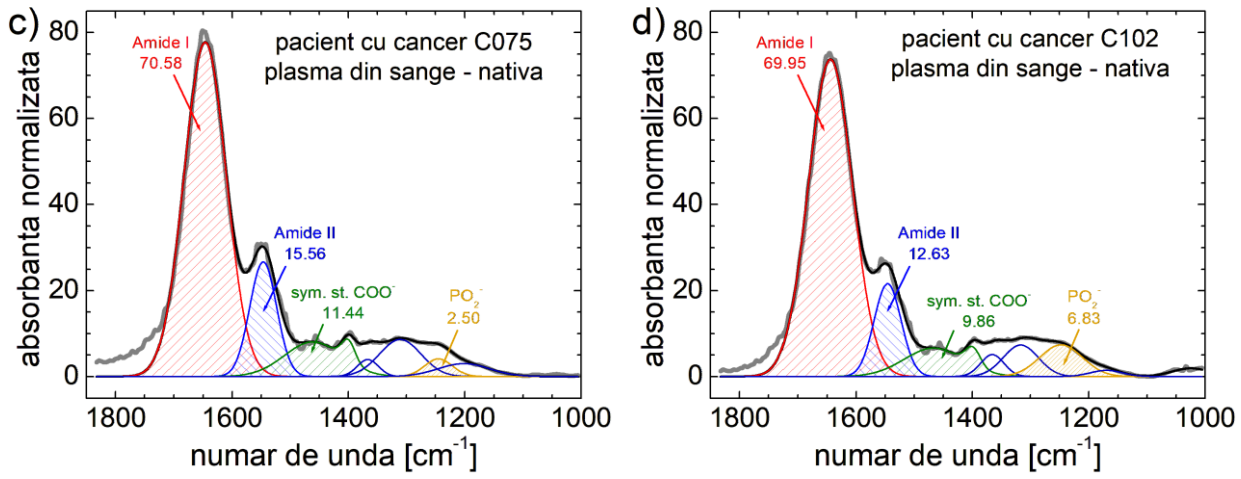

Figura 6.1 Deconvoluția spectrelor FT-IR măsurate pentru plasma nativă colectată de la voluntari sănătoși a) V1 și b) V3 și pentru pacienții cu cancer colorectal c) C075 și d) C102. Sunt prezentate de asemenea ariile integrale corespunzătoare amidei I, Amida II se întinde simetrică a COO^- și $\boldsymbol{PO_2^-}$.

and 6.1d) in the wavenumber range from 1850 $^{cm-1}$ to 1000 $^{cm-1}$. Together with the measured spectrum (gray spectra represented with thicker line), the deconvolution results consisting of a sum of eight Gaussian functions (spectra represented with black lines) as well as each individual Gaussian function (represented with different colors in Figure 6.1) are presented.

Table 6.1 Parameters relevant to principal component analysis, including age, principal self-scattering coefficient, mean values (calculated using equation (6.14)) of the *T2* distribution for blood plasma proteins and for native and deproteinized blood plasma from 1H MRI relaxometry with echo appearance times (TE) of 70 ms, 500 ms and 1000 ms and integrated area calculated from normalized absorbance of FT-IR spectra for amide I and amide II and symmetrical stretch vibrations of chemical bonds in COO- functional groups and assessed for healthy volunteers (V1-V3) and colorectal cancer patients (C075-C103) [34].$\boldsymbol{PO_2^-}$

Sample	Age [years]	D_{main} [$10^{-9}m^2/s$]	$T_{2,av}^{(prot)}$ [ms]	$T_{2,av}^{(nat.\ TE=70)}$ [ms]	$T_{2,av}^{(nat.\ TE=500)}$ [ms]	$T_{2,av}^{(DP\ TE=70)}$ [ms]	$T_{2,av}^{(DP\ TE=1000)}$ [ms]	Amide I	Amide II	Sym. St. COO^-	PO_2^-
V1	52	4.28	3.72	493	588	2971	2807	62.90	9.52	8.43	0.65
V2	57	4.32	3.385	575	615	2779	2685	57.56	7.28	7.18	1.06
V3	47	3.94	1.202	554	578	2712	2679	60.03	8.31	8.80	3.31
C075	70	2.55	1.387	610	665	2473	2476	70.58	15.56	11.44	2.50
C081	43	2.51	0.519	499	610	2561	2530	70.69	11.33	11.12	0.37
C098	73	2.89	0.2091	482	541	2496	2658	61.84	9.18	7.83	1.04
C100	73	2.92	0.1816	687	716	2622	2543	63.73	9.68	15.05	1.96
C101	54	2.95	0.5019	611	694	2643	2578	72.68	9.47	11.34	3.10
C102	66	2.53	0.6587	683	709	2705	2640	69.95	12.63	9.86	6.83
C103	66	2.57	1.469	518	598	2658	2719	61.35	8.40	13.14	2.79

The T2 relaxation time distributions measured by MRI of ^{1H} show a variable number of *peaks* depending on the experimental conditions or the health status of the patients/volunteers. So it was decided to simplify the analytical procedure and eliminate this inconvenience. Therefore, in order to quantify with a single number each distribution of the transverse relaxation time, *T2* that should be used in a PCA analysis was calculated the mean (*T2,av*) using the relationship [34],

$$T_{2,\text{av}} = \frac{\int_0^\infty f(T_2) T_2 dT_2}{\int_0^\infty f(T_2) dT_2,}. \quad (6.14)$$

Calculated T2,av values are presented in Table 6.1, for all volunteers and patients with colorectal cancer for T2 *distributions* measured for native and deproteinized blood plasma and blood plasma proteins. They are also used as input values for statistical analysis in the main components. The age of colorectal cancer volunteers/patients, MRI parameters and FT-IR parameters, which are presented in Table 6.1 are used together for statistical analysis in the main components [29].

6.1.2 PCA analysis results

The main result of the PCA statistical analysis, a scatter plot of PC1 versus PC2 values is shown in Figure 6.2. As mentioned before, PCA analysis involves a special type of graphical representation in which several types of parameters (usually with different units of measurement) can be represented together with the aim of separating data belonging to different groups (classes), but at the same time, if the chosen parameters are relevant, lead to a coagulation (grouping) for data points belonging to the same group [29].

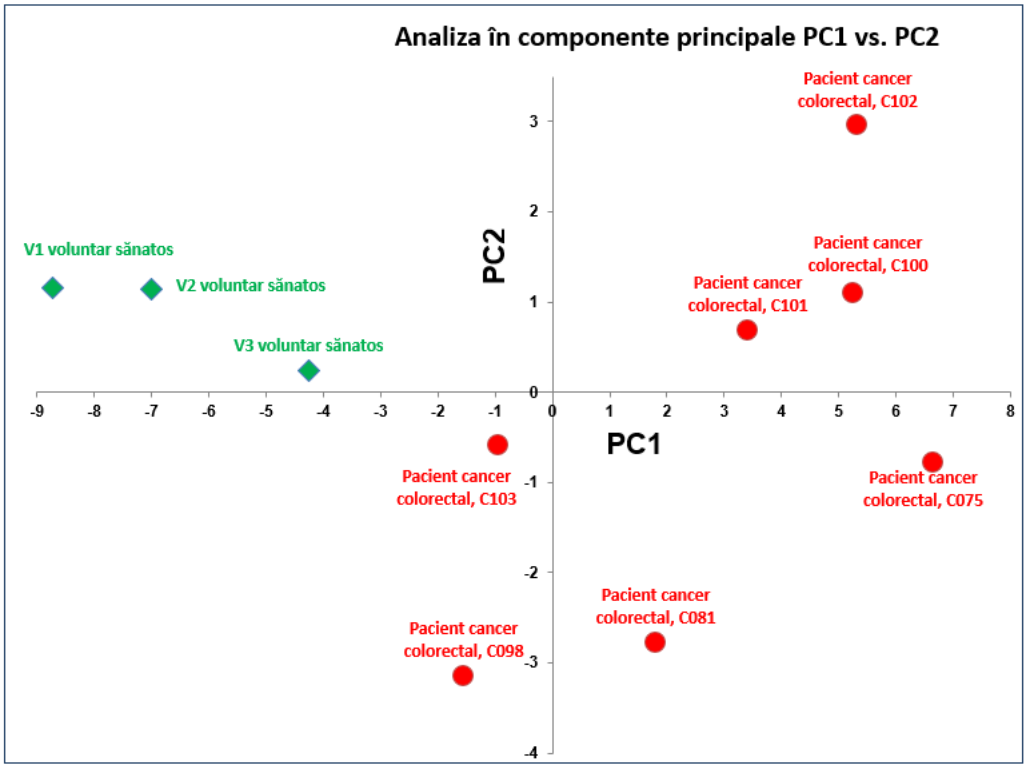

Figure 6.2 PC1 versus PC2 graph from the principal components analysis.

6.2 Analysis of PCA, ROC and AUC values used to assess healing after surgery in patients with colorectal cancer

6.2.1 PCA Analysis

As shown in the previous subchapter, to analyze the effective PCA, of great importance, in addition to the position of *peaks* is the integral area of *peaks*. Such PCA analysis (correlated with ROC and AUC values) applied directly to FT-IR spectra is used to assess healing after surgery in patients with colorectal cancer. In order to quantify the intensity of FT-IR spectra, a different strategy was adopted than the one described above. It has been observed that the deconvolution procedure and quantification of each particular *peak* is time-consuming. Alternatively, a principal component statistical analysis (PCA) can be applied directly to the FT-IR spectra which involves only a transposition of the original data recorded as two columns (the first with the values of the wavenumbers and the second with the absorbance) into a single line representing the measured value of the absorbance of the FT-IR spectrum and the wavenumbers representing the measured parameters. This creates a matrix that has the number of columns equal to the number of measured values for the wavenumbers, and the number of lines is equal to the number of FT-IR spectra measured.

In Figure 6.3a, the evolution from preoperative to postoperative is marked with a dotted arrow for each patient. The arrow is black if the evolution goes from low PC1 values to high PC1 values and red if it goes in the opposite direction. The quantification of the different behaviors in the native blood plasma (Fig. 6.3a) shows: i) a small evolution as in the case of P9 which remains isolated at PC1 and PC2 negative; ii) an evolution towards the cluster of healthy clusters as in the case of P10 and P8; iii) the evolution to a new state (at PC1 and PC2 positive) represented by many postoperative individuals as in the case of P1, P2, P3, P4, P5 and P6; and iv) small evolution to an area of uncertainty as in the case of P7, which (in terms of FT-IR spectra measured for native blood plasma) postoperatively in the first approximation is similar to healthy volunteers V16 and V17 and in the second approximation to preoperative P8 and P2.

În Figura 6.3b se poate observa faptul că un grup mare de simboluri este localizat la valori ale lui PC1 negative este format din voluntari sănătoși, și cazuri preoperatorii și postoperatorii. Se poate observa o altă zonă la numere PC1 pozitive unde avem doar două simboluri preoperatorii aparținând pacienților mai discutați P5 și cei de mai sus identificați ca pacient izolat P9. Componenta PC2 nu pare să fie capabilă să inducă o separare. În PC1, poziția în spectrele FT-IR cu influență mai mare de 90 % se găsește în intervalele de: i) de la ~500 până la ~850 cm^{-1}; ii) de la ~1000 până la 1050 și ~1080 până la 2020 cm^{-1} (aparținând întinderii C-O); iii) de la ~1350 până la ~1600 cm^{-1} (întinderea simetrică a P-O-C, întinderea simetrică a grupurilor funcționale COO- PO_2^- și Amidei II); iv) de la ~ 2000 până la ~2300 cm^{-1} (de multe ori neobservat sau observat ca o

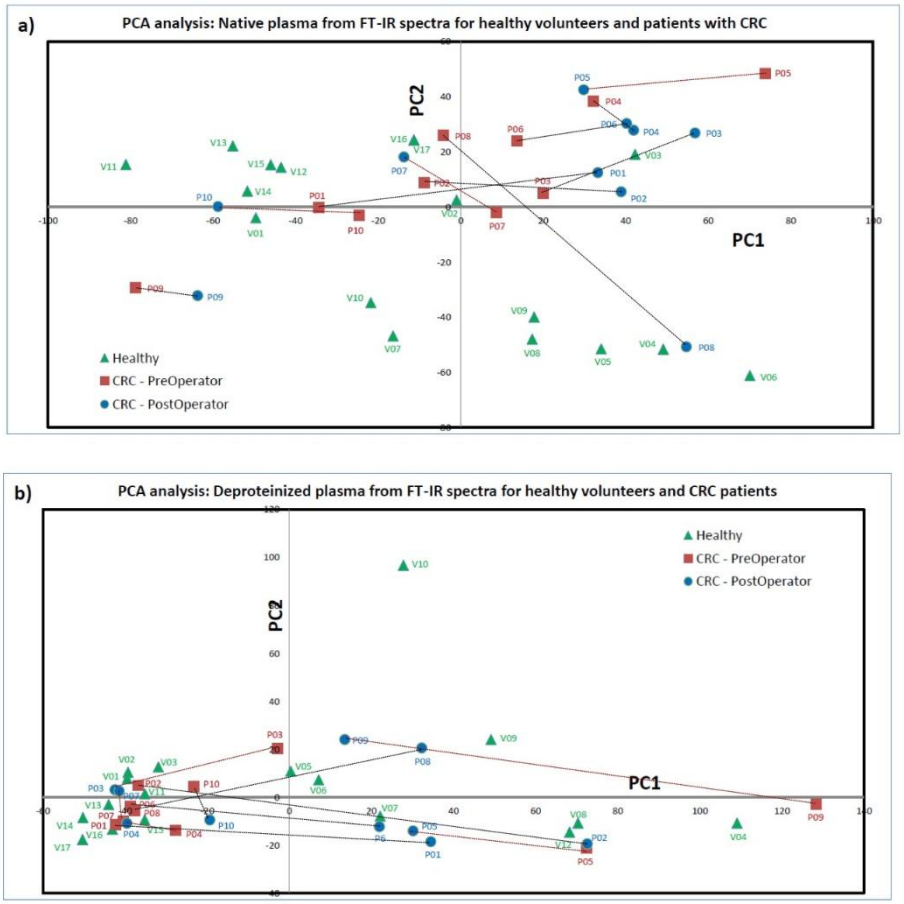

Figure 6.3 PCA analysis of FT-IR spectra measured for a) native and b) deproteinized blood plasma.

combination of restricted rotation and bending of the O-H bond (in water) [248]); and v) from ~2400 to ~ 3700 $^{cm-1}$. Basically, FP1 was influenced by the entire relevant FT-IR spectrum. In this case, several types of developments can be observed: i) small developments within the non-discriminatory area as in the case of P4, P7 and P10; ii) medium developments as in the case of P3 going into the non-discriminatory cluster or P5 entering an area populated by healthy volunteers and postoperative patients; and iii) large developments as in the case of P2, P1, P6 and P8 moving from the non-discriminatory cluster to the healthy zone for healing and P9 moving from the extreme right zone to the healthy zone for healing.

6.2.2 ROC curves and AUC values

Compared to the PCA analyses performed on deproteinized blood plasma, the ROC curves show that the PCA analysis performed on native blood plasma separates the four ad-hoc groups much better. This can be seen from the corresponding AUC, where for PC1 obtained for native blood plasma (see Figure 6.4a) values between 0.576 (native versus colorectal cancer pre – before

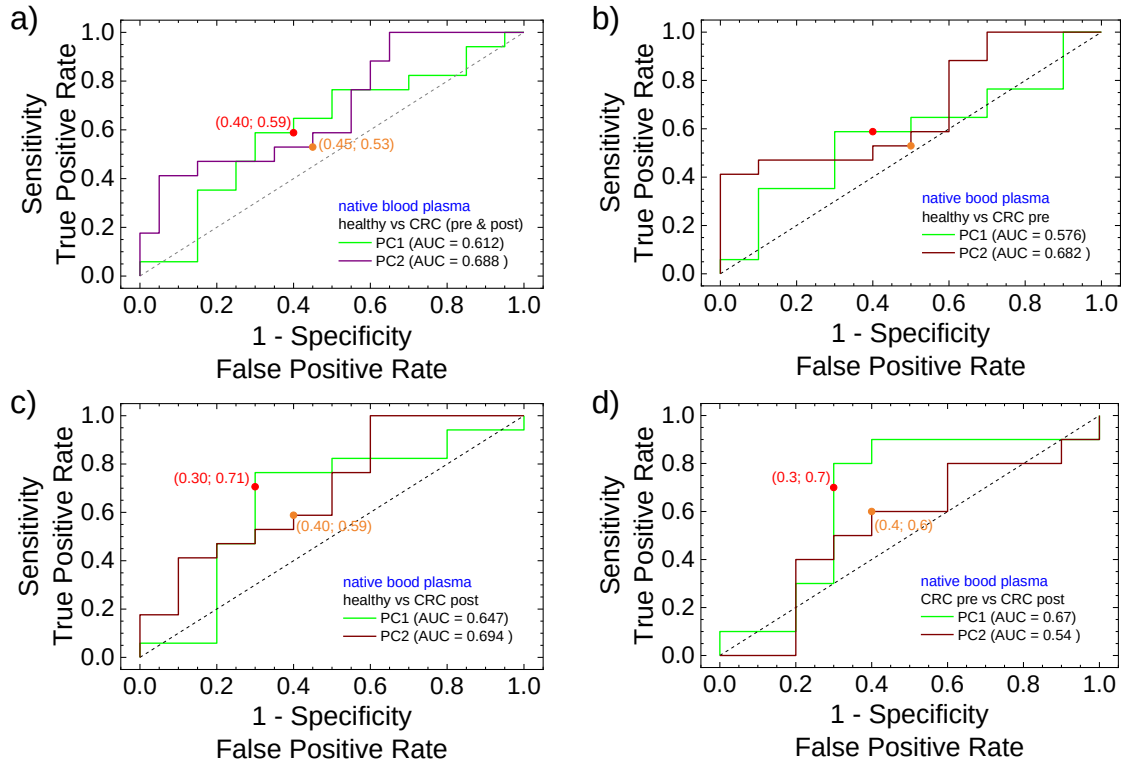

Figure 6.4 ROC curves calculated from PCA analysis data of FT-IR spectra measured for native blood samples for PC1 (green curve) and PC2 (brown curve) taking into account the analyzed pairs: a) healthy (positive) versus CRC (preoperative – preoperative and postoperative – post); b) healthy (positive) versus CRC (preoperative – pre), c) healthy (positive) versus CRC (postoperative – post) and d) CRC (preoperative – pre) (positive) versus CRC (postoperative – post). Optimal *cutting points* are indicated for both PC1 and PC2 parameters. The values of the areas under the curve (AUC) are also indicated.

surgery) and 0.67 (colorectal cancer – pre versus colorectal cancer – postoperatively). The fact that PC1 (with the highest relevance) shows a high AUC value, comparing native blood plasma collected from patients with preoperative and postoperative colorectal cancer indicates that a certain evolution is observed after surgery (here, the optimal *cut-off point* was located at 0.7 sensitivity and 0.3 specificity). The expected prediction was that the clearest separation would be observed between the group of healthy volunteers and the group of patients with preoperative colorectal cancer (with specificity/sensitivity 1 of 0.4/0.6). The highest AUC value (0.694) was obtained for the PC2 component in the evaluation of healthy volunteers versus postoperative colorectal cancer patients. This is a clear indication that the healing process is not oriented towards a state described by healthy volunteers and, in this way, supports, once again, the existence of a *distinct* post-operative state. Unless the analysis of native blood samples taken from preoperative and postoperative colorectal cancer patients is compared, for the rest of the cases, the AUC value measured for PC2 is higher than that measured for PC1.

6.3 PCA Statistical Analysis and Machine Learning Prediction

Comparing the two PC1 versus PC2 representations based on FT-IR spectra measured for native and deproteinized blood plasma (Figures 6.5), only one was chosen for prediction, namely the one resulting from the analysis of native blood plasma. The measured data (PC1 and PC2 coordinates) together with the corresponding label (healthy volunteers, preoperative CRC patients, postoperative CRC patients) constituted the input data with which the virtual machine was trained. After training an artificial neural network constituted virtually using software written for this purpose in JavaScript to which specific libraries were added. Each point in the rectangular area was considered a point in the image space (screen) and the trained artificial neural network was asked to predict the state: healthy, preoperative colorectal cancer or postoperative colorectal cancer. This classification is normalized, so the results for each class come as a probability. Probability maps for all three classes are shown in Figures 6.5.

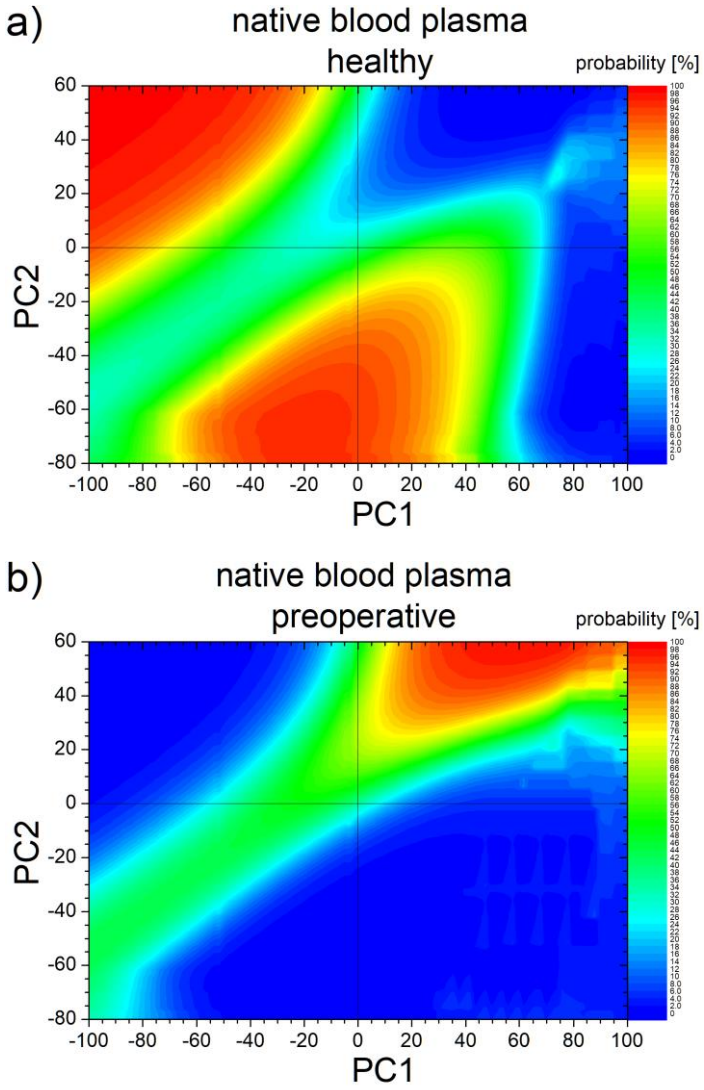

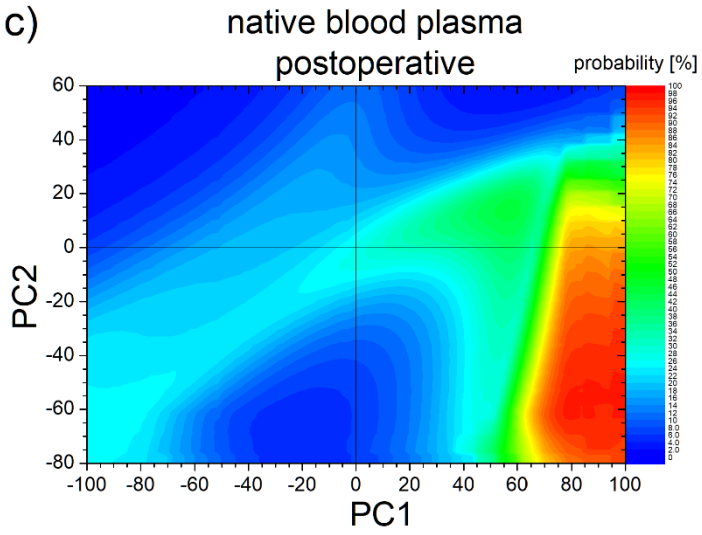

Figure 6.5 Machine learning used to predict the state of a) health; and the probability of CRC b) pre-operative and c) postoperative from the 2D PCA analysis of FT-IR spectra measured for native blood plasma.

The medium probabilities (30 – 70 %) surround the areas with high probability (see green), and the low probability (blue color) is found at high values of PC1 (zone I) and positive values of PC1 and PC2 (zone II). An increased probability (~ 25 %) can be observed compared to the surrounding points, and is found for values of about 70 – 80 for PC1 and 20 – 30 for PC2 due to the presence of V3. We expected an average probability along the entire quasi-diagonal area. The machine learning algorithm predicted an increased probability for positive values of PC1 and large values (> 30) of PC2.

Of real interest was the map predicted and associated with the measurement of FT-IR spectra on native blood plasma collected from colorectal cancer patients 7 days after surgery. This is because in the graph PC1 versus PC2 (see Fig. 6.3a) the points associated with this category do not form a separate cluster. But these points are in the vicinity of the points associated with one or two of the other category. Surprisingly, one can find an isolated area that is characterized by a high probability to locate postoperative patients. This can be found at high PC1 values and negative PC2 values. It is surprising, because in this area we have only one point, belonging to the postoperative P8. Moreover, the V6 is closer to that area than the P8. This artifact is more likely due to incomplete training. The rest of the map is credible and one can find a high probability (~40 – 70 % - green colors) for positive values for PC1 and positive values (up to ~30) for PC2 covering the area called *healing*. As mentioned before, at positive PC1 values (25 – 60) and negative PC2 values, we also have an increased probability (light blue to green) due to the presence of postoperative P8.

CHAPTER 7 IDENTIFICATION OF CANCEROUS COMPONENTS IN BLOOD PLASMA BY HIGH-RESOLUTION MRI SPECTROSCOPY

7.1 Spectrum analysis using the Processing interface and quantification of metabolites

The last step to quantify the metabolites in each MRI spectrum of 1H recorded for blood plasma is to read it (using software written in ProcessingTM) as text, as obtained after export using the jMRUITM software. This software is developed by a group of researchers from the Technical University of Cluj-Napoca, in the last 10 years, and is specially dedicated to the analysis and quantification of the MRI spectra of 1H recorded for tissues (*in vivo* or *ex-vivo*)

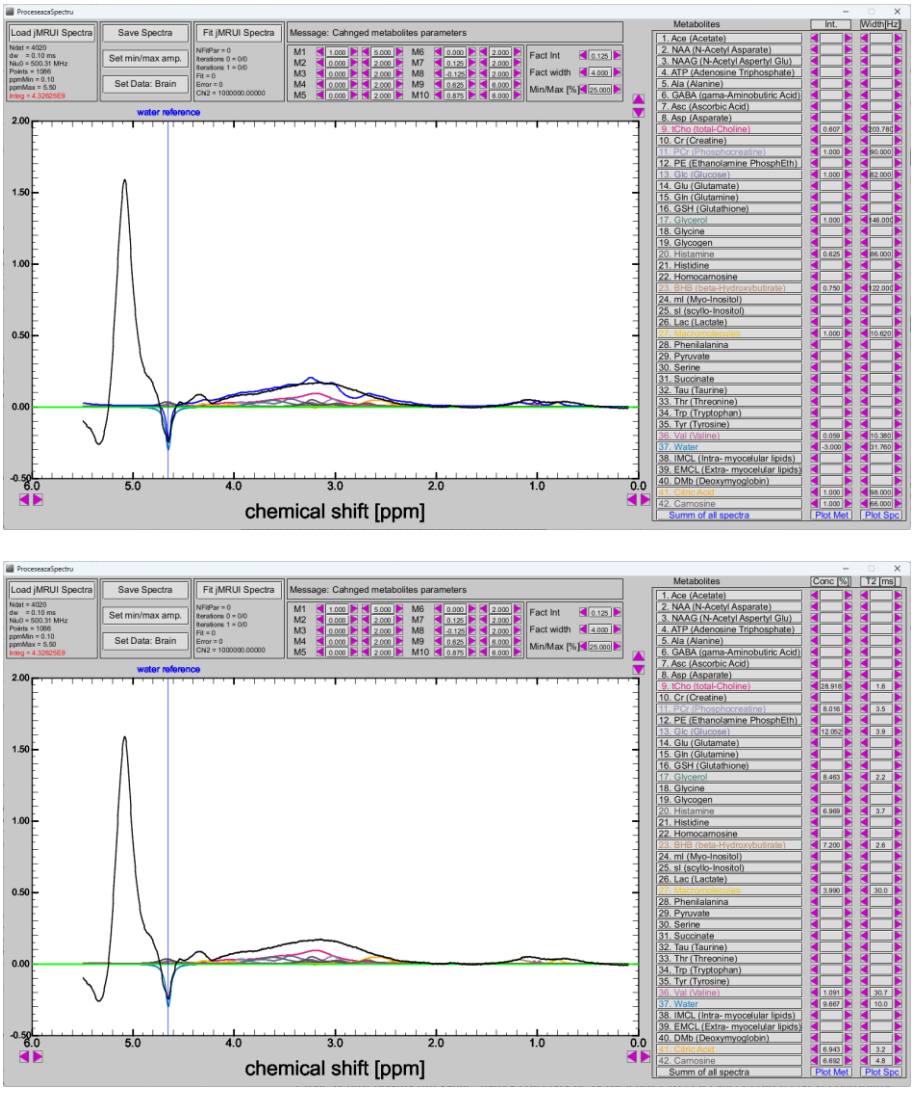

Figura 7.1. Captura de ecran cu fereastra softului Processing care prezintă spectrele RMN a ^{1}H înregistrate pentru plasma din sânge nativă, colectată de la pacienții P105 cu cancer colorectal și contribuția câtorva metaboliții identificați a) intensitate și lărgime de linie și b) concentrație și timpul de relaxare $\boldsymbol{T_2}$.

or biological materials (such as blood or blood plasma) and involving the presence of a large number of metabolites. The NMR spectra of 1H for a total of 41 metabolites and water can be

simulated taking into account the total number of absorption lines and scalar couplings (J) between the nuclear spins. The intensity of each metabolite can be slightly modified, as well as the line width, a parameter that is related to the magnetic field that was used experimentally (its intensity and homogeneity). The effect of homogeneity (i.e. line width) was explored in subchapter 2.1.4, where for a number of metabolites the spectra for a line width at semi-height $\Delta\nu$ = 0.5, 1.0, 2.0 and 4.0 Hz were presented. By pressing a button (*load jMRUI Spectra*) the NMR spectrum of 1H is read from the corresponding file (exported from jMRUI and located in the Input directory of the basic program), and graphically represented with a black curve (see Figures 7·1). In the next step, the limits of spectrum representation (in amplitude and chemical displacement) are chosen. The software allows approximation of data with a sum of individual metabolite spectra using the Levenberg–Marquardt algorithm. To do this, press the *Fit jMRUI Spectra* button. Error and mean squared deviation (χ^2) are the parameters for evaluating the degree of approximation. This algorithm implies that for the values of the approximate parameters, an initial value must be given. And the convergence of the approximation (success rate) is most often conditioned by the choice of a set of values of the best parameters (initial approximation). The number of parameters to be approximated is large, for each metabolite the amplitude (or intensity) of the signal as well as the line width are taken into account. An uninspired choice most of the time leads to a non-convergence of the simulated spectrum to the measured one, but in certain cases it can lead to a divergence involving non-physical values for certain approximate parameters. Thus, for data *protection*, a procedure has been implemented that allows the parameters to vary only by a certain percentage around the initial approximation. Thus, the first step in initiating the approximation of the spectra is to choose, from the list presented in the right menu (see Figures 7.1), each metabolite in turn and to observe if it could be present in the measured spectrum. Metabolites for which the amplitude of the measured spectrum, at the values of the chemical displacements for which they are defined (for all these values), is zero or negligible, are eliminated. This feature, which allows the observation of the NMR spectrum of each metabolite for the entire definition range, is essential and is not implemented in any of the previously described software (ParaVisionTM 360 v3.5, Bruker-TopSpinTM or jMRUITM), which is why they have not been used for quantification of metabolites. Thus, the presence of a metabolite from the measured NMR spectra cannot be affirmed if the spectrum characteristic of the metabolite cannot be presented as a deconvolution for the entire definition range (see Figure 7.7) and not only for single specific values, as presented by, for example, the ParaVision^{TM} 360 v3.5 software.

CHAPTER 8 ADVANCED HIGH-FIELD MRI METHODS FOR THE ANALYSIS OF BIOPSIES HARVESTED FROM COLORECTAL CANCER PATIENTS

8.1 MRI imaging for the evaluation of biopsies taken from the colon and rectum area

8.1.1 T1-encoded MRI images

MRI images of some biopsies are not as spectacular as those recorded for whole organs. Figure 8.2 shows a series of such MRI images acquired as a series of 9 slices in sagittal section, using the *T1-FLASH* protocol, on the 11.7 T MRI tomograph measured 24 hours after biopsy for two tissues from the same colon in the area with cancer – top and healthy – down, collected from

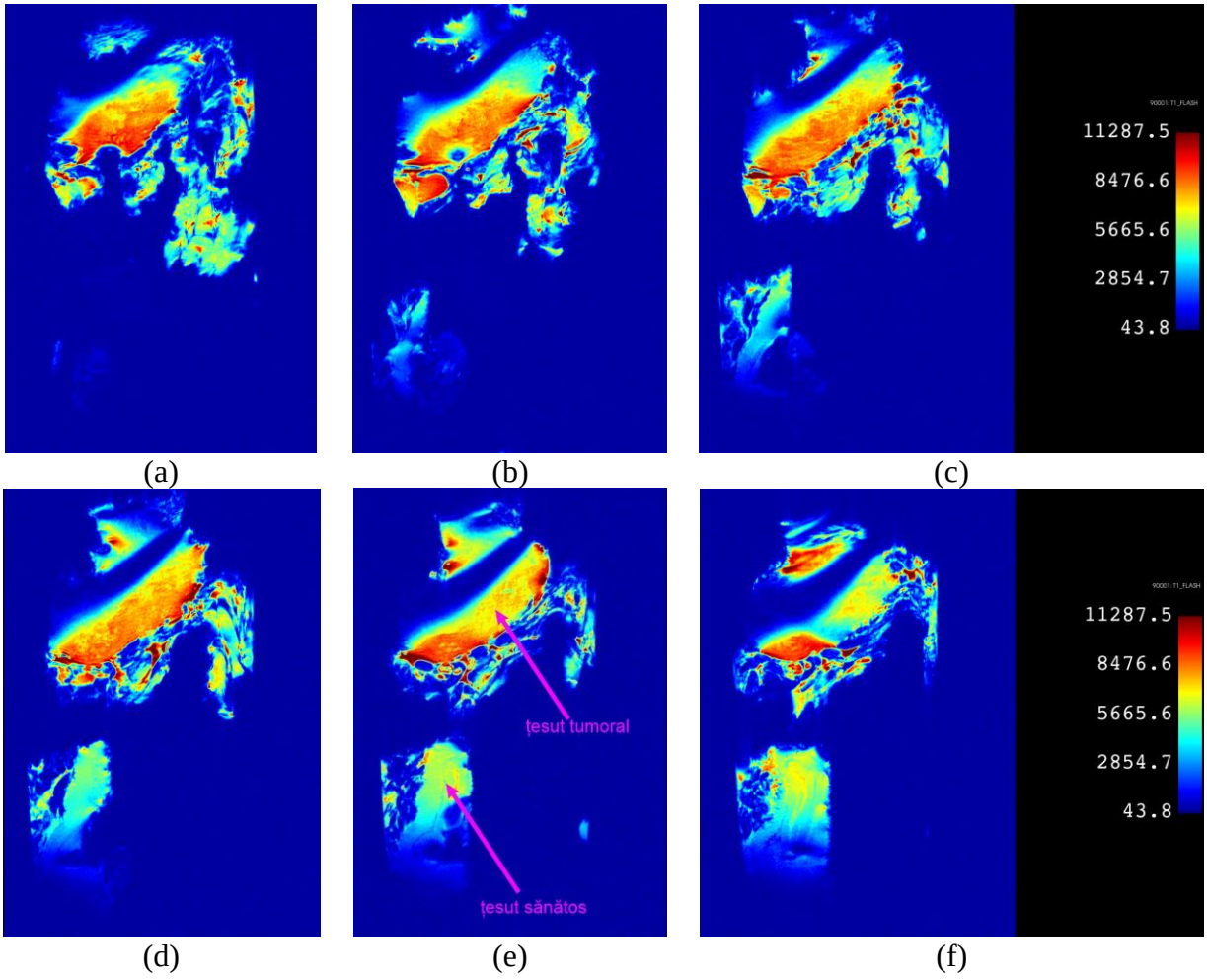

(a) (b) (c)

(d) (e) (f)

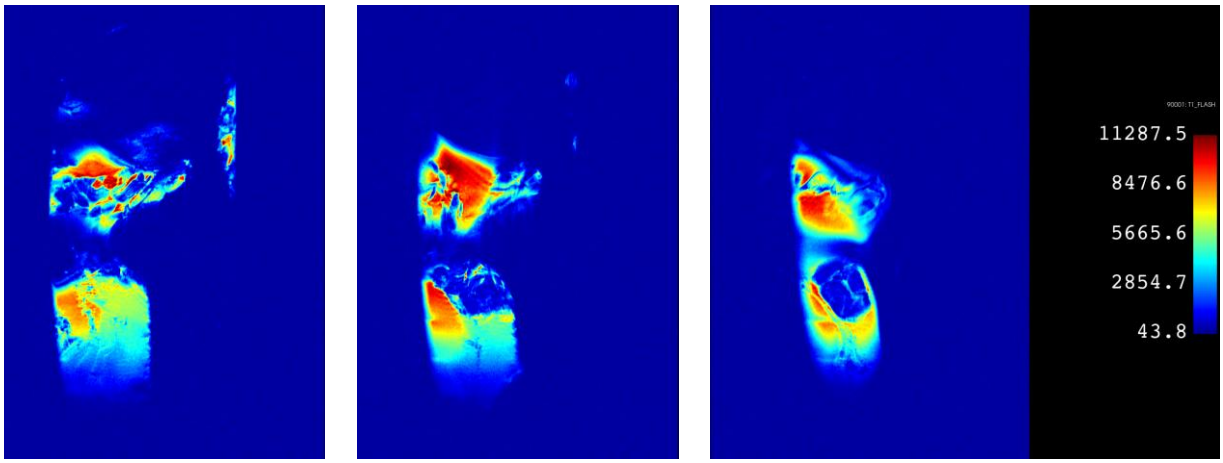

(g) (h) (i)

Figure 8.1. Images of 9 slices coded with T1 longitudinal relaxation time acquired using the *T1-FLASH* protocol at the BioSpec 11.7 T MRI tomograph for two tissues (with cancer – top and healthy – bottom) collected from a cancer patient measured 24 hours after biopsy.

a cancer patient. For a deeper interpretation of the images, it is necessary to know the anatomical components that make up the colon and that can be observed in axial section. Thus, for a complete section of a sigmoid colon (the area of the colon close to the rectum) one could observe the lumen, which is the empty space inside through which fecal matter passes *in vivo*. This component is not visible in the images presented in this chapter because the biopsy did not remove the entire colon. What can be seen in Figure 8.1 is the sigmoid colon wall. It is composed of four main layers: i) the inner layer (which secretes mucus in order to facilitate the passage of fecal matter) is called mucosa; ii) the next layer consists of a connective tissue (which contains blood vessels, lymphatic vessels and nerves) and which is called the submucosa; iii) the mucosa and submucosa are separated by a layer of mucosal musculature; iv) there is also a musculature of its own and which presupposes the existence of a muscular layer responsible for peristalsis (which represents the set of movements of the colon that lead to the movement of waste – fecal matter – to the rectum, and which, at the level of the large intestine, occurs with a reduced frequency of only a few times a day), and which has a circular (internal) and a longitudinal (external) component; v) the outer layer that appears as a serous membrane covering the sigmoid colon is called serous; vi) it is surrounded by the peritoneum; vii) On the outside there is a mesenteric adipose tissue: it surrounds the sigmoid colon and contains blood and lymphatic vessels that supply the colon. If we were to describe the mechanism of cancer invasion, then it can be said that initially, colorectal cancer remains limited to the internal area of the mucosa. Later it can invade the submucosa and the muscle layer. At this point, the risk of metastasis through the lymphatic and blood vessels is increased. In advanced stages, colorectal cancer can invade the serous and peritoneum, reaching the mesenteric vessels and from there to adjacent structures, which can be the bladder and ureters or the uterus in women.

8.1.2 T2-encoded MRI images

The most well-known MRI imaging times are those encoded with the T2 spin-spin relaxation time. Most of the time a small T1 spin-spin relaxation time is associated with a small T2 spin-spin relaxation time (but this is not a rule, especially as in the real case where we do not have a single value for these two relaxation times, *T1* and *T2*, but a distribution of values, indicating the presence of components with complex molecular dynamics). Thus, in MRI images encoded with T2 spin-spin relaxation time, as is the case in Figure 8.2 and which were recorded using the T2-TurboRARE protocol at the 11.7 T BioSpec MRI tomograph, the more intensely colored areas will be described by a high value of T2 spin-spin relaxation time and/or a high value of spin density. In images 8.2a to 8.2f it can be seen that the area of the tumor tissue is represented by bluish colors and that they can be associated with MRI signal values that are up to 25% of the maximum values obtained (in these images – the values are represented as numbers in the internal system of the spectrometer without being able to indicate a more concrete unit of measurement) and that means that both the spin-spin T2 relaxation time, is small and the spin density is relatively (at other areas in the image) low. In contrast, the peripheral areas, which have been associated with the serosa, adipose tissue and blood and lymphatic vessels, are characterized by a high T2 spin-spin relaxation time as well as a high hydrogen density. It has its most likely source in water, which can be found in abundance in these layers of the sigmoid colon. At the same time, from figures 8.2c to 8.2f, it can be seen that healthy tissue is also characterized by MRI signals that are about 20-25% of the maximum values obtained and that can also be associated with a low spin-spin T2 relaxation time as well as with a relatively low spin density (1H). This makes it more difficult to identify colorectal cancer directly from such encoded images, with the T2 spin-spin relaxation time. This would require ignoring (from a practical point of view, saturating the images in the peripheral areas: serous, adipose tissue, and blood and lymphatic vessels) and obtaining improved contrast for the 15-25% areas of the signal. From this point of view, it can be said that the images encoded with the T1 spin-spin relaxation time, (as shown in Figure 8.1 recorded with the *T1-FLASH* protocol) show a better natural contrast (obtained without the use of contrast agents) than the images encoded with the T2 spin-spin relaxation time (as shown in Figure 8.3 and which were recorded using the T2-TurboRARE protocol). Otherwise, from both types of images, certain features can be observed that indicate the texture of the tissues, especially in the internal area of the clone, such as the mucosa and connective tissue. A clear advantage of MRI imaging techniques is that, once the tumor area is identified, it can be very well delimited, and therefore, quantified as spatial extent.

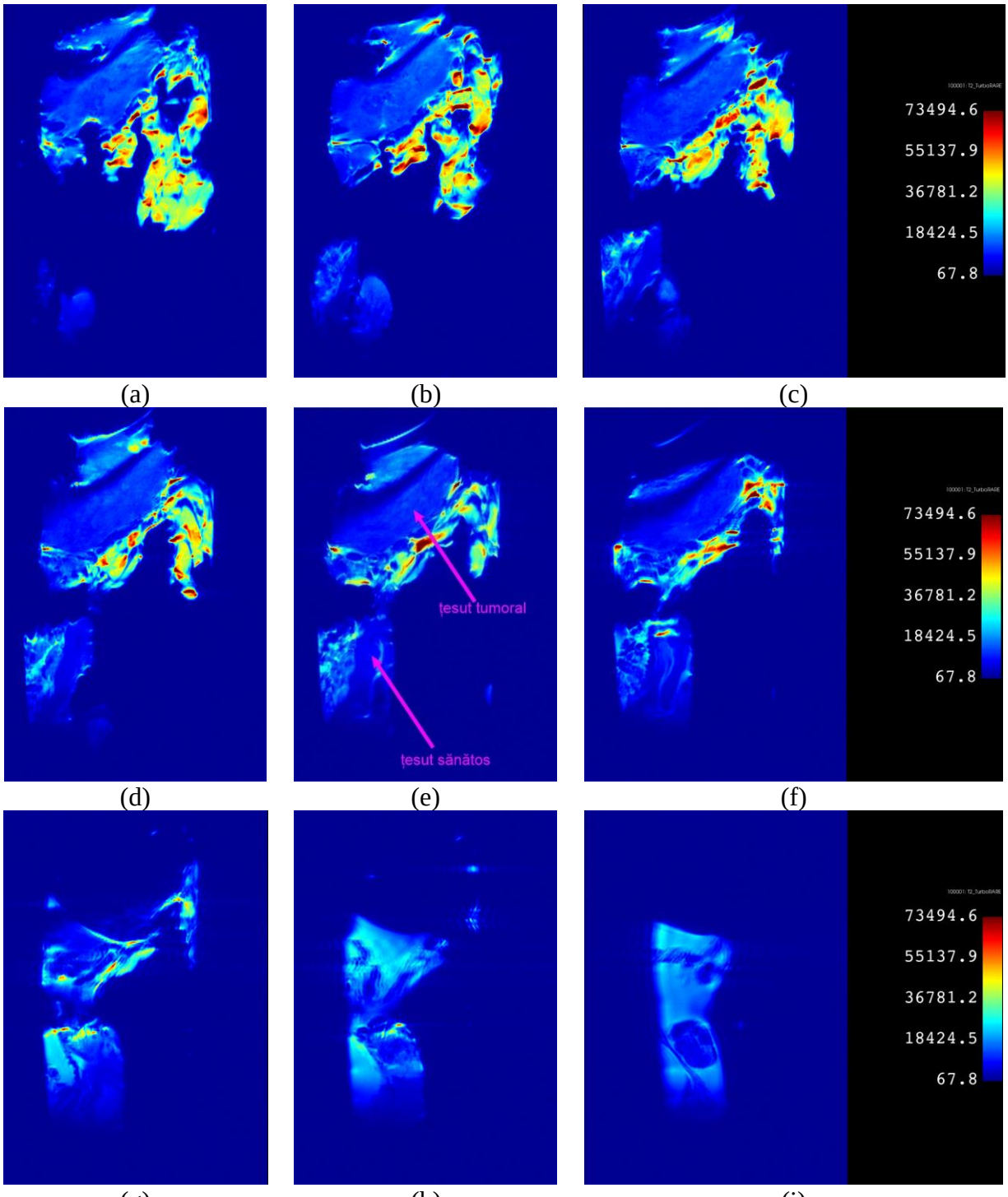

Figure 8.2. Images of 9 slices coded with T2 longitudinal relaxation time acquired using the T2-TurboRARE protocol at the BioSpec 11.7 T MRI tomograph for two tissues (with cancer – top and healthy – bottom) collected from a cancer patient, measured 24 hours after biopsy.

8.2. MRI spectroscopy of tumor tissue biopsy

In the MRI spectrum of high-resolution 1H recorded in high fields (11.7 T) for tumor tissue, the presence of several metabolites is observed in addition to the spectrum recorded for healthy tissue. First of all, peaks with (relatively) high amplitudes, located at ~ 1.1 ppm and ~

0.67 ppm as well as the series of peaks with lower amplitude, located in the range from ~ 1.7 ppm to ~ 3.3 ppm, are observed. Secondly, it was observed that the quantification results in a higher number of metabolites (to which macromolecules and water are added), which obviously lead to a change in the concentration as follows: i) water (~41.4 %↓); ii) adenosine triphosphate (ATP) (~11.38%↓); iii) macromolecules, especially M1, M2 and M9 (~8.86 %↑); iv) alanine (0 %↓); v) valine (~14.83 %↑); vi) intracellular lipids (0 %↓); vii) ascorbic acid (~1.28 %↑); viii) glucose (0%↓); ix) lactate (~1.91 %↑); to which are added a number of new metabolites:

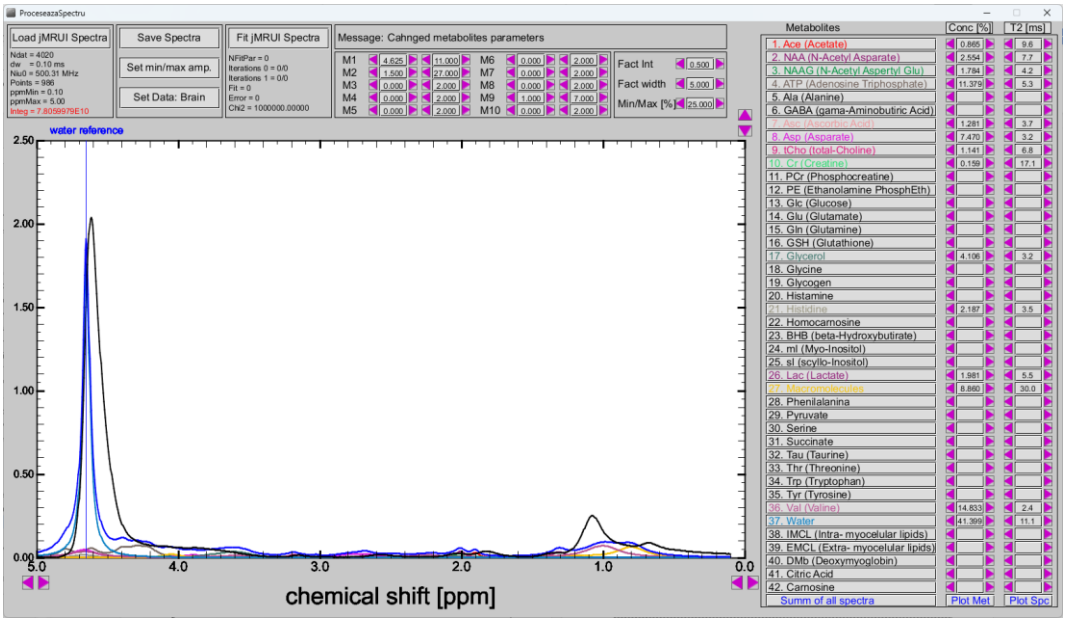

Figura 8.3. Screenshot of the Processing software window showing the MRI spectra of 1H recorded for tumor tissue collected from a colorectal cancer patient and the contribution of several identified metabolites, their concentrations and *T2* relaxation time.

x) asparat (~7.47 %↑); xi) glycerol (~4.11 %↑); xii) NAA (N-acetyl asparate) (~2.55 %↑); xiii) histidine (~2.19 %↑); xiv) NAAG (N-acetyl aspertyl glutamate) (~1.78 %↑); xv) total choline (~1.14 %↑); xvi) acetate (~0.87 %↑) and xvii) creatinine (~0.16 %↑). The estimated T2 relaxation time for macromolecules remained the same (30 ms) but increased for water (11.1 ms). Otherwise, in general, T2 relaxation time values have values between 2.4 ms (valine) and 9.6 ms (acetate), indicating a slight narrowing of the absorption lines in the MRI spectrum of 1H of high resolution recorded for tumor tissue biopsy.

8.3 High-field MRI relaxometry

8.3.1 T2 distributions obtained for tumor and healthy tissue biopsies

In the lower-right half are shown the CPMG drops obtained using the Bruker ParaVision 360 v3.5 software that operates the BioSpec 11.7 T MRI spectrometer. They were obtained from the sequence of 64 images recorded for a biopsy of a tissue (affected by colorectal cancer and a resection margin) located in the colon area. Along with the experimental data, the statistical errors

(mean values and the statistically obtained mean square deviation for all the voxels that make up each area of interest) are presented, as well as the approximation with a mono-exponential function (the only one available for the Bruker ParaVision 360 v3.5 software). Single values of *T2* relaxation times, measured for tumor tissue () and healthy tissue (). In the lower-central part there is a map (map) obtained as a value of the relaxation times $T_2^{\text{tumoare}} = 17.70\ msT_2^{\text{sănătos}} = 19.99\ msT2$, measured in each voxel.

From the analysis of the approximation curves (fitting) of the experimental data, it is observed that these approximation can be characterized as deficient. Thus, it is necessary to implement another method of approximation of experimental data and which has been presented in the experimental program of this thesis, namely the analysis of CPMG curves using the inverse Laplace transform. The spin-spin relaxation time distributions of the 2 CPMG curves presented are comparatively represented in Figure 8.4. It is observed that tissues (both tumor and healthy) are characterized not by a dynamic component (as would result from the primary Bruker ParaVision analysis) but by 4 components with different molecular dynamics.

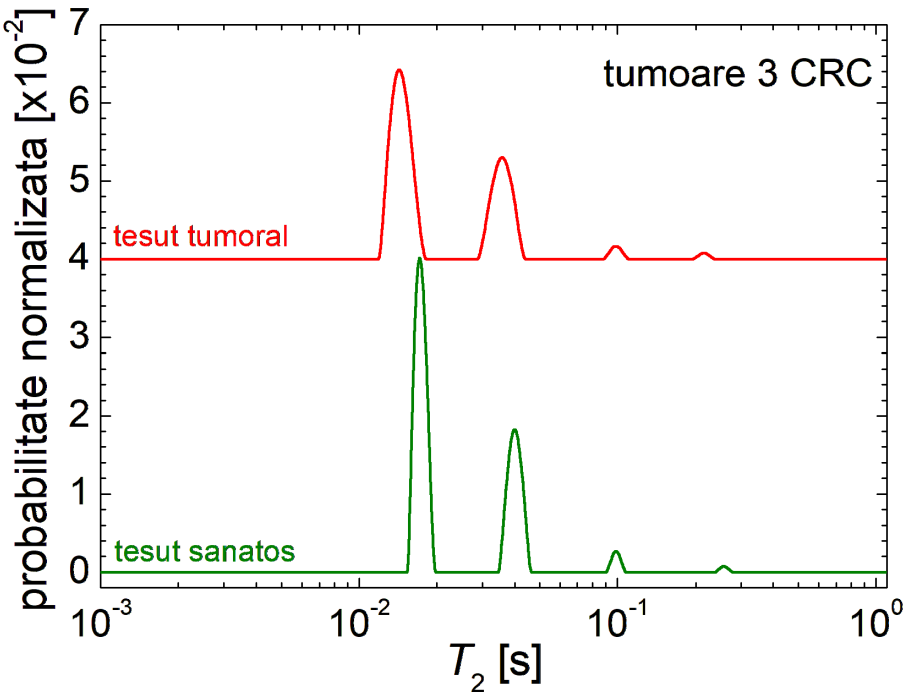

Figure 8.4. T2 relaxation time distributions measured by MRI of ^{1H} recorded in high magnetic fields (*ex-vivo*) for biopsy of a tumor tissue (red) and a healthy marginal tissue (green), both collected from a colorectal cancer patient.

8.3.2 Mape parametrice de T_2 obținute pentru biopsii ale țesutului tumoral și sănătos

The ultimate goal of MRI relaxometry studies using images recorded in high fields is to aT2 parametric maps obtained for biopsies of tumor and healthy tissue obtain parametric maps containing information about the location in space of the various *component parts* (tissues,

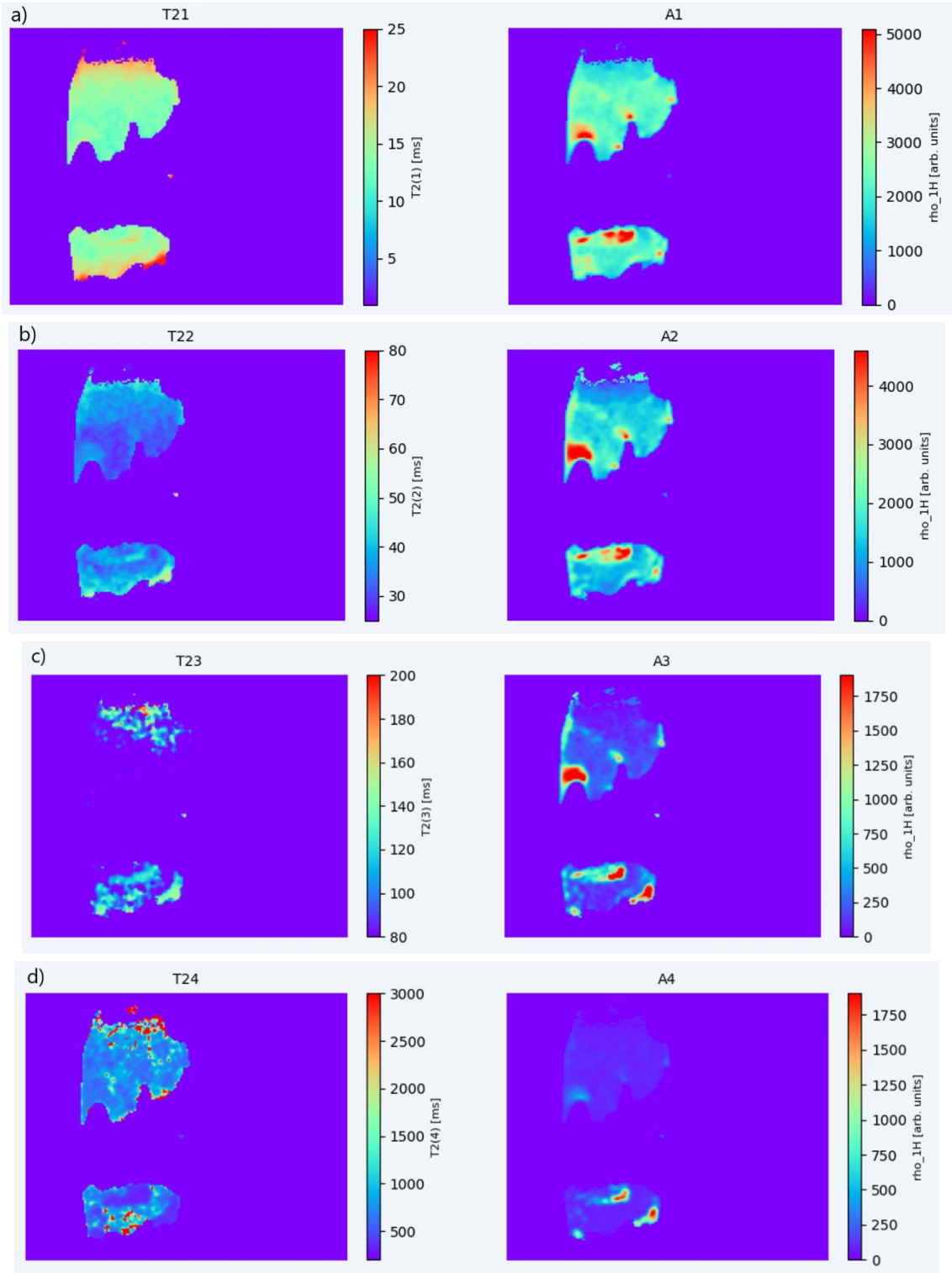

Figure 8.5. Parametric maps representing the spatial distributions of *T2* relaxation time and spine density (1H) measured by MRI of 1H recorded in high magnetic fields (*ex-vivo*) from the echo train drop shown in Figure 8.7 for biopsy of a tumor tissue and a healthy marginal tissue, both collected from a colorectal cancer patient.

subsections of tissues, tissues with various characteristics – for example tumors) by obtaining a more relevant contrast between the area of interest and the adjacent areas.

CONCLUSIONS

1. A research plan was developed with the aim of performing a complex characterization of materials with biological origins such as fluids (blood plasma) and human tissues, both from patients diagnosed with colorectal cancer and from healthy subjects in the control group.

2. The selection criterion for colorectal cancer patients and healthy volunteers included in the study was rigorously defined, for which both relevant clinical and biological aspects and their compatibility with the research objectives were considered. The recruitment process involved the detailed evaluation of the medical history, biological parameters and inclusion and exclusion criteria, thus ensuring the validity and relevance of the results obtained.

3. Modern methods of relaxometry and diffusiometry MRI of 1H in low magnetic fields have been successfully used for the characterization of blood plasma (native, deproteinized as well as plasma proteins), being initially applied to a small batch of samples in a pilot study, and later extended to a larger batch of samples, in order to obtain more robust and representative results in an extended study.

4. It has been shown that the main values of the self-diffusion coefficient, *D* can be successfully used to differentiate native plasma biological samples from colorectal cancer patients from healthy volunteers.

5. FT-IR spectroscopy proved to be an effective method for complex characterization of the same blood plasma components, being initially applied to the same small batch of samples in the pilot study, and later extended to a larger batch, in order to validate and consolidate the results obtained.

6. It has been demonstrated that modern methods of 1H MRI relaxometry and FT-IR spectroscopy applied to sets of blood plasma samples from patients with colorectal cancer can be successfully used to assess the degree of cure at 7 days after surgery and, if correlated with statistical and machine learning methods, can be used as methods to predict healing after surgery.

7. The complex data analysis was a detailed procedure that involved the implementation of several steps, starting from the primary processing of the raw data obtained by FT-IR spectroscopy measurements and 1H MRI relaxometry and diffusiometry , followed by the Fourier transform and the inverse Laplace transform to obtain the Fourier or Laplace spectra

(spin-spin relaxation time distributions, *T2* or the self-diffusion coefficient, *D*) as well as their deconvolutions. In the quantitative analysis stage, statistical tools were used to evaluate and interpret the parametric values and spectra obtained. Finally, the process was completed with advanced statistical analysis, using the principal component analysis (PCA) technique, which was improved by integrating artificial intelligence algorithms. This included the use of artificial neural networks and machine learning techniques to identify patterns and extract meaningful insights from complex datasets.

8. The PCA analysis applied to native blood plasma provides a significantly clearer separation of the four groups formed *ad-hoc*, compared to the similar analysis performed on deproteinized blood plasma, as indicated by the ROC curves. This idea has also been expressed by the 1H MRI diffusiometry measurements showing that for differentiating the specific characteristics of colorectal cancer, there is no need to use deproteinized plasma that requires a longer preparation time, additional technique, and reagents that can lead to an increase in the complexity of the measured spectra correlated with an increase in the difficulty of interpretation.

9. It has been proposed to use MRI spectroscopy of 1H in high fields (7 T and 11.7 T) to identify cancer-associated components in blood plasma, allowing a detailed and precise analysis of the metabolites present. This advanced method provided valuable insights into the specific metabolic changes associated with the presence of cancer cells.

10. MRI imaging, spectroscopy and relaxometry of 1H in high fields has been successfully used for the analysis of biopsies harvested from patients with colorectal cancer, allowing the identification and characterization of metabolic compounds in tumor tissues and healthy tissue, thus contributing to the accurate diagnosis and deeper understanding of the pathological processes associated with this disease.

BIBLIOGRAPHY

1. Z. Guleken, H. Bulut, G. I. Gültekin, S. Arıkan, I. Yaylım, M. T. Hakan, D. Sonmez, N. Tarhan, and J. Depciuch, "Assessment of structural protein expression by FT-IR and biochemical assays as biomarkers of metabolites response in gastric and colon cancer," Talanta, vol. 231, p. 122353, 2021..
2. E. Morgan, M. Arnold, A. Gini, V. Lorenzoni, C. J. Cabasag, M. Laversanne, J. Vignat, J. Ferlay, N. Murphy, and F. Bray, "Global burden of colorectal cancer in 2020 and 2040: incidence and mortality estimates from GLOBOCAN," *Gut*, vol. 72, no. 2, pp. 338–344, 2023, doi: 10.1136/gutjnl-2022-327736.
3. F. Islami, A. Goding Sauer, K. D. Miller, R. L. Siegel, S. A. Fedewa, E. J. Jacobs, M. L. McCullough, A. V. Patel, J. Ma, I. Soerjomataram, W. D. Flanders, O. W. Brawley, S. M. Gapstur, and A. Jemal, "Proportion and number of cancer cases and deaths attributable to potentially modifiable risk factors in the United States," CA Cancer J. Clin., vol. 68, no. 1, pp. 31–54, 2018, doi: 10.3322/caac.21440.
4. M. Bretthauer, M. Løberg, P. Wieszczy, M. Kalager, L. Emilsson, K. Garborg, M. Rupinski, E. Dekker, M. Spaander, M. Bugajski, Ø. Holme, A. G. Zauber, N. D. Pilonis, A. Mroz, E. J. Kuipers, J. Shi, M. A. Hernán, H. O. Adami, J. Regula, G. Hoff, M. F. Kaminski, and the NordICC Study Group, "Effect of colonoscopy screening on risks of colorectal cancer and related death," N. Engl. J. Med., vol. 387, no. 17, pp. 1547–1556, 2022, doi: 10.1056/NEJMoa2208375
5. N. H. Kim, M. Y. Lee, J. H. Park, D. I. Park, C. I. Sohn, K. Choi, and Y. S. Jung, "Serum CEA and CA 19-9 levels are associated with the presence and severity of colorectal neoplasia," *Yonsei Med. J.*, vol. 58, no. 5, pp. 918–924, 2017, doi: 10.3349/ymj.2017.58.5.918
6. Shaukat and T. R. Levin, "Current and future colorectal cancer screening strategies," *Nat. Rev. Gastroenterol. Hepatol.*, vol. 19, no. 8, pp. 521–531, 2022, doi: 10.1038/s41575-022-00612-y
7. K. Rogers, *Blood; Physiology and Circulation (The Human Body)*, Britannica Educational Publishing, New York, NY, USA: 29 East 21st Street, 2010.
8. J. Schaller, S. Gerber, U. Kaempfer, S. Lejon, și C. Trachsel, *Human Blood Plasma Proteins: Structure and Function*. Chichester, West Sussex, England: John Wiley & Sons Ltd, 2008.
9. K. Saladin, *Anatomy & Physiology: The Unity of Form and Function*. New York, NY, USA: McGraw-Hill Science/Engineering/Math, 2003

10. J. E. Hall, *Guyton and Hall Textbook of Medical Physiology: Enhanced E-book*. Saunders, 2010
11. J. D. Potter și D. Hunter, *Genetics of Colorectal Cancer*, N. M. Lindor și J. D. Potter, Eds. 1st ed. New York, NY, USA: Springer-Verlag, 2009.
12. H. Sung, J. Ferlay, R. L. Siegel, M. Laversanne, I. Soerjomataram, A. Jemal și F. Bray, "Global cancer statistics 2020: GLOBOCAN estimates of incidence and mortality worldwide for 36 cancers in 185 countries," *CA Cancer J. Clin.*, vol. 71, no. 3, pp. 209–249, 2021, doi: 10.3322/caac.21660
13. A. Jemal, T. Murray, E. Ward, A. Samuels, R. C. Tiwari, A. Ghafoor, E. J. Feuer și M. J. Thun, "Cancer statistics, 2005," *CA Cancer J. Clin.*, vol. 55, no. 1, pp. 10–30, Jan.–Feb. 2005, doi: 10.3322/canjclin.55.1.10.
14. C. Dervenis și E. Xynos, *Colorectal Cancer: Special Issue: Digestive Diseases 2007*. Basel, Switzerland: S. Karger Pub, 2007
15. B. Vogelstein, E. R. Fearon, S. R. Hamilton, S. E. Kern, A. C. Preisinger, M. Leppert, Y. Nakamura, R. White, A. M. Smits și J. L. Bos, "Genetic alterations during colorectal-tumor development," *N. Engl. J. Med.*, vol. 319, no. 9, pp. 525–532, Sep. 1988, doi: 10.1056/NEJM198809013190901.
16. D. A. Wirtzfeld, N. J. Petrelli și M. A. Rodriguez-Bigas, "Hamartomatous polyposis syndromes: Molecular genetics, neoplastic risk, and surveillance recommendations," *Ann. Surg. Oncol.*, vol. 8, pp. 319–327, 2001.
17. H. T. Lynch și C. A. de la Chapelle, "Hereditary colorectal cancer," *N. Engl. J. Med.*, vol. 348, pp. 919–932, 2003.
18. G. Xie, X. Ma, A. Zhao, C. Wang, Y. Zhang, D. Nieman, și J. K. Nicholson, "Metabolic profiling of human plasma by ultra-performance liquid chromatography/mass spectrometry,"J.Chromatogr.B, vol. 927, pp. 15-20, 2013. DOI: 10.1016/j.jchromb.2013.03.007
19. R. A. de Graaf, *In Vivo NMR Spectroscopy: Principles and Techniques*, 3rd ed. Chichester, U.K.: Wiley, Dec. 2018.
20. R. I. Chelcea, R. Fechete, E. Culea, D. E. Demco, și B. Blümich, "Distributions of transverse relaxation times for soft-solids measured in strongly inhomogeneous magnetic fields," J. Magn. Reson., vol. 196, no. 2, pp. 178–190, 2009, doi: 10.1016/j.jmr.2008.11.004.
21. L. Venkataramanan, Y. Q. Song, și M. D. Hürlimann, "Solving Fredholm integrals of the first kind with tensor product structure in 2 and 2.5 dimensions," IEEE Trans. Signal Process., vol. 50, pp. 1017–1026, 2002.

22. M. D. Hürlimann și L. Venkataramanan, “Quantitative measurement of two-dimensional distribution functions of diffusion and relaxation in grossly inhomogeneous fields,” J. Magn. Reson., vol. 157, pp. 31–42, 2002.
23. Y. Q. Song, L. Venkataramanan, M. D. Hürlimann, M. Flaum, P. Frulla, și C. Straley, “T_1–T_2 correlation spectra obtained using a fast two-dimensional Laplace inversion,” J. Magn. Reson., vol. 154, pp. 261–268, 2002.
24. K. E. Washburn și P. T. Callaghan, “Propagator resolved transverse relaxation exchange spectroscopy,” J. Magn. Reson., vol. 186, pp. 337–340, 2007
25. G. C. Borgia, R. J. S. Brown, și P. Fantazzini, “Uniform-penalty inversion of multiexponential decay data,” J. Magn. Reson., vol. 132, pp. 65–77, 1998.
26. M. D. Hürlimann, M. Flaum, L. Venkataramanan, C. Flaum, R. Freedman, și G. J. Hirasaki, “Diffusion-relaxation distribution functions of sedimentary rocks in different saturation ratios,” Magn. Reson. Imaging, vol. 21, pp. 305–310, 2003.
27. M. Hürlimann, L. Burcaw, și Y. Q. Song, “Quantitative characterization of food products by two-dimensional D–T_2 and T_1–T_2 distribution functions in a static gradient,” J. Collo-id Interface Sci., vol. 297, pp. 303–311, 2006.
28. S. Godefroy și P. T. Callaghan, “2D relaxation/diffusion correlations in porous me-dia,” Mag. Reson. Imaging, vol. 21, pp. 337–340, 2003.
29. R. Fechete, I. A. Morar, D. Moldovan, R. I. Chelcea, R. Crainic, and S. C. Nicoară, "Fourier and Laplace-like low-field NMR spectroscopy: The perspectives of multivariate and artificial neural networks analyses," *J. Magn. Reson.*, vol. 324, p. 106915, 2021. https://doi.org/10.1016/j.jmr.2021.106915.
30. S. K. Sharma, D. S. Verma, L. U. Khan, S. Kumar, and S. B. Khan, Eds., Handbook of Materials Characterization. Cham, Switzerland: Springer, 2018
31. S. Aştilean, Metode şi tehnici moderne de spectroscopie optică, Vol. 1: Spectroscopia IR şi Raman, Cluj-Napoca, România: Editura Casa Cărţii de Ştiinţă, 2002.
32. U. Barlev, O. Zelig, C. Bar, S. Segev, S. Mordechai, J. Kapelushnik, I. Nathan, F. Flomen, H. Kashtan, R. Dickman, O. Madhala-Givon, and N. Wasserberg, "A novel method for screening colorectal cancer by infrared spectroscopy of peripheral blood mononuclear cells and plasma," *J. Gastroenterol.*, vol. 51, pp. 214–221, 2016.
33. **L. R. Șaitiș**, D. Andras, I. A. Pop, C. Șaitiș, R. Crainic, and R. Fechete, "Spectroscopic nuclear magnetic resonance and Fourier transform-infrared approach used for the evaluation of healing after surgical interventions for patients with colorectal cancer: A pilot study," *Cancers (Basel)*, vol. 17, no. 5, p. 887, Mar. 2025. doi: 10.3390/cancers17050887.

34. **L. R. Drăgan**, D. Andras, and R. Fechete, "Fourier Transform Infrared (FT-IR) Spectroscopy and Proton Nuclear Magnetic Resonance (^{1}H NMR) Relaxometry and Diffusometry for the Identification of Colorectal Cancer in Blood Plasma," *Anal. Lett.*, vol. 56, no. 2, pp. 286–302, 2023, doi: 10.1080/00032719.2022.2065497.

LIST OF PUBLICATIONS IN THE FIELD OF THE THESIS

Papers published in ISI journals

1. **Lavinia Raluca Dragan**, David Andras, Radu Fechete, Fourier Transform Infrared (FT-IR) Spectroscopy and Proton Nuclear Magnetic Resonance (^{1}H NMR) Relaxometry and Diffusometry for the Identification of Colorectal Cancer in Blood Plasma, Analytical Letters, 56 (2), 286-302, (2023) https://doi.org/10.1080/00032719.2022.2065497 (IF: 1.6, AIS: 0.267).
2. Ramona Crainic, A. S.Farcașanu, P. Păscuță, **L. R. Șaitiș**, F. Popa, Radu Fechete, Complex Characterization of Nanofiber Biomaterials Based on Chitosan, Collagen and Fish Gelatine Produced by Electrospinning." *Analytical Letters* (2024): 1-29: https://doi.org/10.1080/00032719.2024.2372348 (IF: 1.6, AIS: 0.267).
3. **Lavinia Raluca Șaitiș**, David Andras, Ioana-Alina Pop, Cătălin Șaitiș, Ramona Crainic and Radu Fechete, Spectroscopic Nuclear Magnetic Resonance and Fourier Transform – InfraRed approach used for the evaluation of healing after surgical interventions for patients with Colorectal Cancer. A pilot study, Cancers Cancers 2025, 17, 887. https://doi.org/10.3390/cancers17050887 (IF: 4.5, AIS: 1.148).
4. **Lavinia Raluca Șaitiș**, Ovidiu Susu, Brigitta Lőrincz, David Andras, Remus Sebastian Sipos, Simion Simon and Radu Fechete, 11.7 T High field Magnetic Resonance Imaging, Spectroscopy and Relaxometry used for the assessment of colorectal tumor biopsy, (Cancers, in preparation).
5. **Lavinia Raluca Șaitiș**, Brigitta Lőrincz, David Andras, and Radu Fechete, High field NMR spectroscopy of blood plasma for the assessment of colorectal cancer, (in preparation).
6. **Lavinia Raluca Șaitiș**, Brigitta Lőrincz, David Andras, and Radu Fechete, Fourier Transform Infrared (FT-IR) Spectroscopy and Proton Nuclear Magnetic Resonance Relaxometry, Principal Component Analysis and Machine Learning used for the evaluation of colorectal cancer from blood plasma, (in preparation).

Papers presented at international conferences

1. **Lavinia Raluca Saitis**, David Andras, Alexandru Stefan Farcasanu, Cătălin Saitis, Ramona Crainic, and Radu Fechete, Integrating Spectroscopic and Imaging Approaches for Improved Biological Fluids and Tissues Biopsy Analysis in Colorectal Cancer

Detection., 33th Anual Conference of the European Society for Biomateriales ESB, 4-8 September 2023, Davos, Switzeland. – Poster.

2. **L R Dragan**, D Andras, Ioana A. Pop, A Farcasanu, C. Saitis, R. Crainic and R Fechete, Spectroscopic NMR and FT-IR approach used for the evaluation of healing after surgical interventions for patients with Colorectal Cancer, 13th biennial International Conference on Processes in Isotopes and Molecules PIM-INCDTIM, 19-22 September 2023, Cluj-Napoca, Romania - Poster.

LIST OF PUBLICATIONS OUTSIDE THE FIELD OF THE THESIS

Papers published in ISI indexed journals

1. **L. R. Dragan**, E. Jumate, C. Aciu, D. L. Manea, R. Fechete, Advanced characterization of plastering mortars with glass waste additives, AIP Conference Proceedings 2206 (1), 030005, (2020).
2. Catalin Saitis, Daniela Lucia Manea, Monica Luminita Plesa; **Raluca Lavinia Saitis**, Recycling, Plaster Waste as a Substitute for Aggregates in Obtaining Plastering, Mortars. Buildings 2023, 13, 491. https://doi.org/10.3390/buildings13020491.

Papers published in non-ISI journals

1. **Lavinia R. Dragan**, Ramona Crainic, Radu Fechete, A comparative study for natural degradation of three local anesthetic drugs for human use by ^{1}h nmr relaxometry and ft-ir spectroscopy. Studia Universitatis Babes-Bolyai, Physica 63, 61-73 (2018).
2. Ramona Crainic, **Lavinia R. Dragan**, Radu Fechete ,^{1}H NMR relaxometry and ATR-FT-IR spectrosopy used for the assesment of wastewater treatment in slaughterhouse, studia universitatis babes-bolyai, physica 63, 49-60 (2018).

Papers presented at international conferences

1. **L. R. Dragan**, E. Jumate, C. Aciu, D. L. Manea and R Fechete, Advanced characterization of plastering mortars with glass waste additives, 12th biennial International Conference on Processes in Isotopes and Molecules PIM-INCDTIM, 25-27 September 2019, Cluj-Napoca, Romania - Poster.
2. R. Fechete, R. Crainic, **L R. Dragan**, D. Moldovan, R. I. Chelcea, The perspectives of numerical neuroevolution of artificial neural networks with applications to Fourier and Laplace-like spectroscopy, 14th biennial International Conference on Processes in Isotopes and Molecules PIM-INCDTIM, 19-22 September 2023, Cluj-Napoca, Romania - Poster.
3. Ramona Crainic, Alexandru Stefan Farcasanu, Petru Pascuta, **Lavinia Raluca Saitis**, and Radu Fechete, Advanced experimental and numeric simulation method used for the characterization of nanofibers biomaterials produced by electrospinning. 33th Anual

Conference of the European Society for Biomateriales ESB2023, 4-8 September 2023, Davos, Switzeland - Poster.